Libraries and Learning Services

University of Auckland Research Repository, ResearchSpace

Copyright Statement

The digital copy of this thesis is protected by the Copyright Act 1994 (New Zealand).

This thesis may be consulted by you, provided you comply with the provisions of the Act and the following conditions of use:

- Any use you make of these documents or images must be for research or private study purposes only, and you may not make them available to any other person.
- Authors control the copyright of their thesis. You will recognize the author's right to be identified as the author of this thesis, and due acknowledgement will be made to the author where appropriate.
- You will obtain the author's permission before publishing any material from their thesis.

General copyright and disclaimer

In addition to the above conditions, authors give their consent for the digital copy of their work to be used subject to the conditions specified on the Library Thesis Consent Form and Deposit Licence.

MODELLING THE FORM AND FUNCTION OF THE TRAPEZIOMETACARPAL JOINT

Marco Tien-Yueh Schneider

Supervised by: Dr Thor Besier, Prof. Poul Nielsen, and Dr Kumar Mithraratne

A thesis submitted in complete fulfilment of the requirements for the degree of Doctoral of Philosophy in Bioengineering, University of Auckland, 2017

Abstract

The trapeziometacarpal (TMC) joint is involved in over 80 % of activities of daily living. However, the joint is susceptible to degradation and osteoarthritic degeneration which can impair the upper extremity by up to 50 %, profoundly affecting the quality of life.

The aetiology of TMC osteoarthritis is poorly understood, but biomechanical factors are implicated at its pathogenesis. The aim of this work was to create a computational framework to investigate the relationship between TMC morphology, kinematics, and cartilage stress distributions in men and women with and without degenerative disease.

We developed a statistical shape model of the TMC joint, an automatic 3D segmentation tool, a parametric population finite element model, and a shape model classifier. These tools can be combined to create an automatic pipeline for predicting cartilage stress and strain from CT data. The framework was used to: characterise the morphology in healthy TMC joints as a function of sex and age, classify cartilage stress distributions across three tasks as a function of sex and age, and characterise the morphological differences between healthy and early osteoarthritic TMC joints.

Our findings showed that there is little variation in morphology of the TMC joint with sex, but suggested that size may play a role in osteoarthritis. From our finite element model, we found that women exhibited higher variation in joint contact, suggesting greater variability in neuromuscular control of thumb joint kinematics. Furthermore, we found a subset of men and women that exhibited peak cartilage stresses in regions with frequent cartilage wear, suggesting that cartilage degeneration may occur through divergent

mechanisms. Our classifier showed that early morphologic changes were present at the volar beak of the first metacarpal and throughout the trapezial articular surface in early osteoarthritic joints, and showed promise for a future diagnostic tool. These methods can be combined to create a pipeline that predicts cartilage stress and strain from CT images.

These findings contribute towards understanding the normal biomechanics of the TMC joint and the aetiology of TMC osteoarthritis.

Acknowledgements

This thesis represents a conclusion to a chapter of my life that was exhilarating, yet challenging, but overall, it has been a period where I have experienced the most personal growth to date. For this I am thankful, and would like to acknowledge the following people who have enriched my experience.

I would first like to thank my supervisors: Thor Besier, Poul Nielsen, and Kumar Mithraratne, for giving me the opportunity to work on this project. I was very lucky to receive the guidance and generosity of three of the greatest supervisors. Thor, thank you for your contagious enthusiasm, kindness, compassion, and support. You have been an amazing mentor, and I could not have imagined a better supervisor. Poul, thank you for sharing your immense knowledge, and for your thorough review of my work. Your meticulous attention to detail is a quality I admire and your passion for science inspires me. Kumar, your mastery of finite element modelling is astounding. Your support in this key area of the thesis was truly appreciated.

I would like to acknowledge the people that collaborated with me on this project. My advisory committee: Joseph Crisco, Amy Ladd, and Arnold-Peter Weiss, were continuously supportive, provided insightful comments, research ideas, and encouragement. This research would not have been possible without their assistance. Tarpit Patel and Eni Halilaj, provided me with technical support and helped me understand variances in the data. Cameron Walker kindly kept his door open to provide me with statistics and analysis advice. In particular, I would like to express deep gratitude to Ju Zhang for collaborating with me, providing feedback on papers, and sharing his wealth of knowledge in

statistical shape modelling and image analysis. Ju, your kindness, openness and willingness to help are qualities that I aim to reciprocate and pay forward on to others.

I would like to thank several people and groups at the ABI: The musculoskeletal modelling group for their kindness and comradery, especially Mousa Kazemi, for his sympathy and help with FEBio; Geoff Handsfield, for the many discussions we've had and for sharing his knowledge on assertion-evidence style of academic presentation; Ted Yeung, for his advice on local coordinate systems and figure advice; Xiao-Ming Wang, for the many in depth, yet open ended discussions; and Dharshini Sreenivasan, for her advice on thesis structure. I would like to acknowledge Nathan Brantly for his genuine kindness and for introducing me to some funky music, and Helen Liley, my desk partner, for sharing many tea and toast sessions with me, listening to my frustrations, inviting me on epic tramping trips, and for keeping me sane. Furthermore, I would like to acknowledge the ABI indoor soccer group, for many great games, and the ABI social committee and Friday drinks committee, for the fun mid-winter BYOs, Friday drinks, and hangouts at OGH. I must not forget the surf crew, especially Geoff Handsfield, Sam Richardson, Daniel Xu, Markus Haller, for the many beautiful and humbling surf sessions.

Finally, I would like to acknowledge my family and friends outside of the ABI for their love and support. My parents have done all they can throughout their lives to ensure my success. To my partner Lisa, thank you for everything, especially your kindness, love, empathy, patience, and way of life.

Table of Contents

List of Figures

LIST OF FIGURES

List of Abbreviations

ASM   active shape model

BFGS   Broyden–Fletcher–Goldfarb–Shanno

CT   computed tomography

FE   finite element

LDA   linear discriminant analysis

OA   osteoarthritis

PC   principal component

PCA   principal component analysis

RF   random forest

RFRV   random forest regression voting

RMS   root mean squared

SED   strain energy density

SSM   statistical shape model

TMC   trapeziometacarpal

Co-Authorship Form

This form is to accompany the submission of any PhD that contains published or unpublished co-authored work. **Please include one copy of this form for each co-authored work**. Completed forms should be included in all copies of your thesis submitted for examination and library deposit (including digital deposit), following your thesis Acknowledgements. Co-authored works may be included in a thesis if the candidate has written all or the majority of the text and had their contribution confirmed by all co-authors as not less than 65%.

Please indicate the chapter/section/pages of this thesis that are extracted from a co-authored work and give the title and publication details or details of submission of the co-authored work. Chapter 2, reproduced from "Automatic segmentation of the thumb trapeziometacarpal joint using parametric statistical shape modelling and random forest regression voting". CMBBE. In review.	
Nature of contribution by PhD candidate	Study design, implementation, analysis, wrote the manuscript.
Extent of contribution by PhD candidate (%)	90

CO-AUTHORS

Name	Nature of Contribution
Ju Zhang	Initial study concept, technical support, edited the manuscript.
Joseph J. Crisco	Collection of data, feedback on manuscript.
Arnold-Peter C. Weiss	Collection of data, clinical expertise.
Amy L. Ladd	Collection of data, clinical expertise.
Poul M. F. Nielsen	Supervision, edited the manuscript.
Thor Besier	Initial study concept, supervised the project, edited the manuscript.

Certification by Co-Authors

The undersigned hereby certify that:
❖ the above statement correctly reflects the nature and extent of the PhD candidate's contribution to this work, and the nature of the contribution of each of the co-authors; and
❖ that the candidate wrote all or the majority of the text.

Name	Signature	Date
Ju Zhang		26-04-2017
Joseph J. Crisco		21-04-2017
Arnold-Peter C. Weiss		23-04-2017
Amy L. Ladd		01-05-2017
Poul M. F. Nielsen		2017-04-25
Thor Besier		25-04-2017

Co-Authorship Form

This form is to accompany the submission of any PhD that contains published or unpublished co-authored work. **Please include one copy of this form for each co-authored work**. Completed forms should be included in all copies of your thesis submitted for examination and library deposit (including digital deposit), following your thesis Acknowledgements. Co-authored works may be included in a thesis if the candidate has written all or the majority of the text and had their contribution confirmed by all co-authors as not less than 65%.

Please indicate the chapter/section/pages of this thesis that are extracted from a co-authored work and give the title and publication details or details of submission of the co-authored work. Chapter 3, reproduced from "Men and women have similarly shaped carpometacarpal joint bones". Journal of Biomechanics. 2015.	
Nature of contribution by PhD candidate	Study design, implementation, analysis, wrote the manuscript.
Extent of contribution by PhD candidate (%)	90
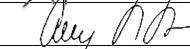
CO-AUTHORS

Name	Nature of Contribution
Ju Zhang	Developed analytical tools, technical support, edited manuscript.
Joseph J. Crisco	Initial study concept, collection of data, feedback on manuscript.
Arnold-Peter C. Weiss	Collection of data, clinical expertise.
Amy L. Ladd	Initial study concept, collection of data, clinical expertise.
Poul M. F. Nielsen	Supervision, feedback on manuscript.
Thor Besier	Initial study concept, supervised the project, edited the manuscript.

Certification by Co-Authors

The undersigned hereby certify that:

❖ the above statement correctly reflects the nature and extent of the PhD candidate's contribution to this work, and the nature of the contribution of each of the co-authors; and

❖ that the candidate wrote all or the majority of the text.

Name	Signature	Date
Ju Zhang		26-04-2017
Joseph J. Crisco		21-04-2017
Arnold-Peter C. Weiss		23-04-2017
Amy L. Ladd		01-05-2017
Poul M. F. Nielsen		2017-04-25
Thor Besier		25-04-2017

Co-Authorship Form

This form is to accompany the submission of any PhD that contains published or unpublished co-authored work. **Please include one copy of this form for each co-authored work**. Completed forms should be included in all copies of your thesis submitted for examination and library deposit (including digital deposit), following your thesis Acknowledgements. Co-authored works may be included in a thesis if the candidate has written all or the majority of the text and had their contribution confirmed by all co-authors as not less than 65%.

Please indicate the chapter/section/pages of this thesis that are extracted from a co-authored work and give the title and publication details or details of submission of the co-authored work.
Chapter 4, reproduced from "Trapeziometacarpal joint contact varies between men and women during three isometric functional tasks". CMBBE. In review.

Nature of contribution by PhD candidate	Study design, implementation, analysis, wrote the manuscript.
Extent of contribution by PhD candidate (%)	90
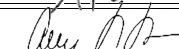
CO-AUTHORS

Name	Nature of Contribution
Ju Zhang	Initial study concept, technical support, edited the manuscript.
Joseph J. Crisco	Collection of data, feedback on manuscript.
Arnold-Peter C. Weiss	Collection of data, clinical expertise.
Amy L. Ladd	Collection of data, clinical expertise.
Kumar Mithraratne	Supervision, FE expertise, edited the manuscript.
Poul M. F. Nielsen	Supervision, edited the manuscript.
Thor Besier	Initial study concept, supervised the project, edited the manuscript.

Certification by Co-Authors

The undersigned hereby certify that:
- ❖ the above statement correctly reflects the nature and extent of the PhD candidate's contribution to this work, and the nature of the contribution of each of the co-authors; and
- ❖ that the candidate wrote all or the majority of the text.

Name	Signature	Date
Ju Zhang		26-04-2017
Joseph J. Crisco		21-04-2017
Arnold-Peter C. Weiss		23-04-2017
Amy L. Ladd		01-05-2017
Kumar Mithraratne		27-04-2017
Poul M. F. Nielsen		2017-04-25
Thor Besier		25-04-2017

Co-Authorship Form

This form is to accompany the submission of any PhD that contains published or unpublished co-authored work. **Please include one copy of this form for each co-authored work**. Completed forms should be included in all copies of your thesis submitted for examination and library deposit (including digital deposit), following your thesis Acknowledgements. Co-authored works may be included in a thesis if the candidate has written all or the majority of the text and had their contribution confirmed by all co-authors as not less than 65%.

Please indicate the chapter/section/pages of this thesis that are extracted from a co-authored work and give the title and publication details or details of submission of the co-authored work. Chapter 5, reproduced from "Early morphologic changes in trapeziometacarpal joint bones with osteoarthritis". Osteoarthritis and Cartilage. In review.	
Nature of contribution by PhD candidate	Study design, implementation, analysis, wrote the manuscript.
Extent of contribution by PhD candidate (%)	90
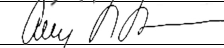
CO-AUTHORS

Name	Nature of Contribution
Ju Zhang	Developed analytical tools, feedback on manuscript.
Joseph J. Crisco	Initial study concept, collection of data, feedback on manuscript.
Arnold-Peter C. Weiss	Collection of data, clinical expertise.
Amy L. Ladd	Initial study concept, collection of data, clinical expertise.
Poul M. F. Nielsen	Supervision, edited the manuscript.
Thor Besier	Initial study concept, supervised the project, edited the manuscript.

Certification by Co-Authors

The undersigned hereby certify that:
❖ the above statement correctly reflects the nature and extent of the PhD candidate's contribution to this work, and the nature of the contribution of each of the co-authors; and
❖ that the candidate wrote all or the majority of the text.

Name	Signature	Date
Ju Zhang		26-04-2017
Joseph J. Crisco		21-04-2017
Arnold-Peter C. Weiss		23-04-2017
Amy L. Ladd		01-05-2017
Poul M. F. Nielsen		2017-04-25
Thor Besier		25-04-2017

Chapter 1.

Introduction

This chapter introduces the central topic of this thesis. The functional anatomy of the healthy carpometacarpal or trapeziometacarpal (TMC) joint is first presented, followed by an overview of osteoarthritic degeneration of the TMC joint. Previous methods for studying TMC joint osteoarthritis (OA) are critically reviewed before the objectives and hypotheses of this thesis are presented. Finally, the novel contributions and research outputs are outlined.

1.1 Motivation

The TMC joint is involved in over 80 % of activities of daily living (Katz et al., 1970). Through the evolution of mankind, the TMC joint has adapted a unique morphology that is responsible for the dexterity, strength, and range of tasks that the hand can perform (Ladd et al., 2014). From playing the piano, to grasping a hammer, therein lies a delicate balance between stability and mobility (Ladd et al., 2013). However, the cost of this marvel is a susceptibility to joint degradation and osteoarthritic degeneration (Ladd et al., 2014), ultimately leading to pain and joint dysfunction (Halilaj et al., 2014d). In severe cases, surgical excision of the trapezium remains the only treatment option for removing pain and recovering joint function (Ladd et al., 2013). The onset of OA in the TMC joint is poorly understood. Biological and biomechanical mechanisms play a role in TMC OA, and although biomechanics is thought to

be the primary factor (Figure 1.1), the aetiology of this disorder remains unclear. Nonetheless, altered stress and strain in the cartilage tissue is believed to play an important role in the onset, progression, and severity of the disease (Conconi et al., 2014, Najima et al., 1997). This thesis addresses a small part of this problem from a biomechanical view point and investigates the relationship between morphology and contact mechanics of the TMC joint (Figure 1.2).
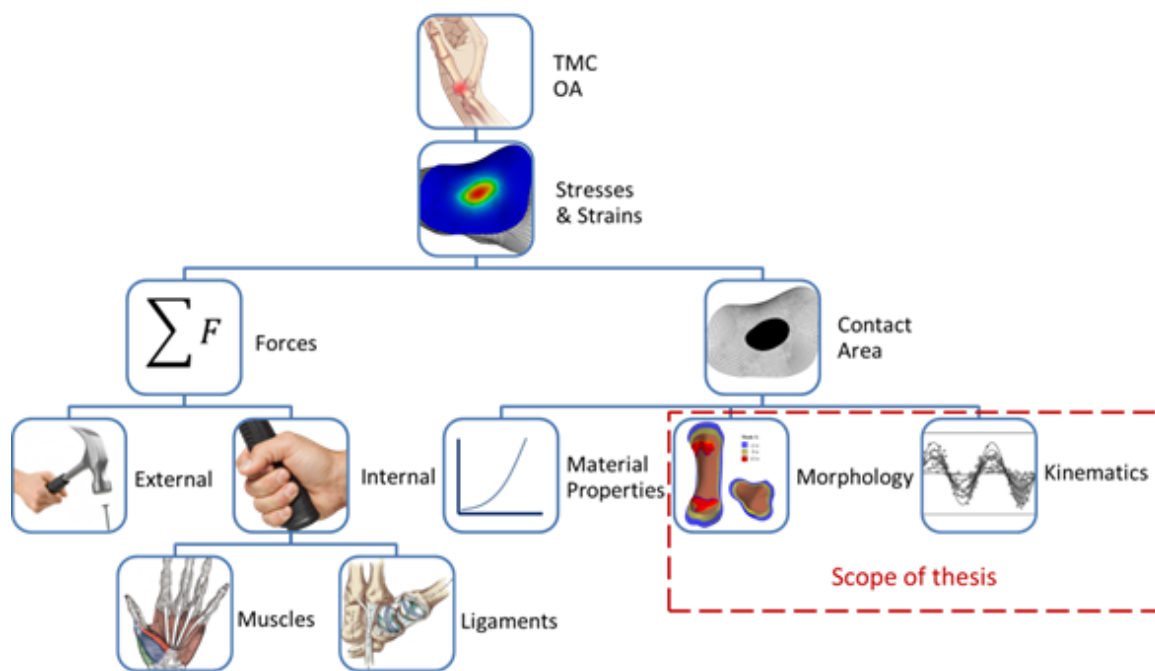
Figure 1.1. Biomechanical factors involved in TMC OA.
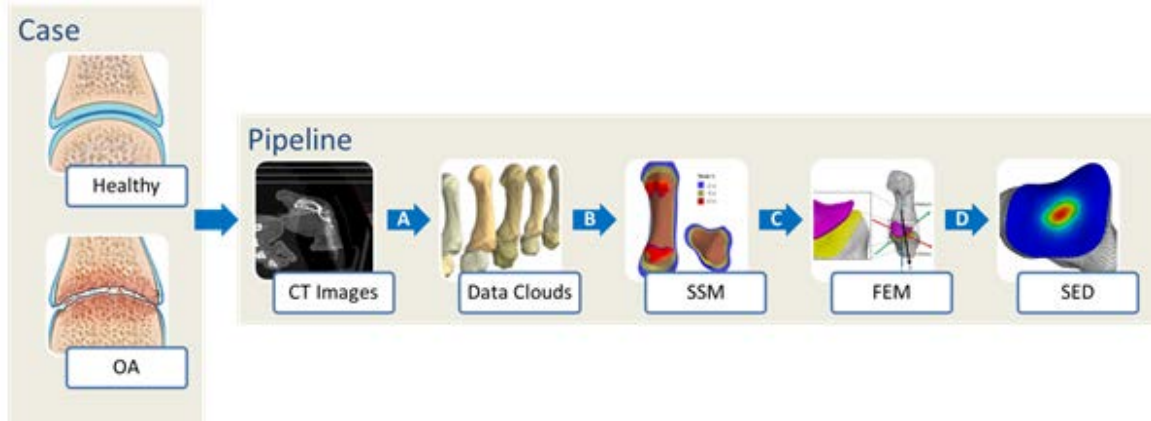
Figure 1.2. Pipeline for analysing TMC joint morphology and its effect on cartilage stress. Segmentation of CT images (A) is followed by the creation of a statistical shape model (SSM) (B). A population FE model is created (C) and stress distributions are calculated for the population (D). We propose to apply this pipeline to understand healthy and osteoarthritic TMC joint morphology and cartilage stress.

1.2   TMC joint anatomy

The TMC joint, also known as the first carpometacarpal joint or basal thumb joint, is the located at the proximal end of the thumb where the first metacarpal articulates with the carpal trapezium in the wrist (Figure 1.3). Functionally, it behaves similarly to a universal or ball joint owing to its unique biconcavoconvex morphology, where the two saddle-shaped bones (Figure 1.4) interlock reciprocally. The base of the first metacarpal is concave in the dorsovolar axis and convex in the radioulnar axis, while the trapezial surface is convex dorsovolarly and concave radioulnarly (Figure 1.3). The saddles are shallow and incongruent in the resting position due to disparate radii of curvature, but become stable and congruent at the extremes of motion (Edmunds, 2011, Haara et al., 2004). For example, screw home torque rotation at the end of opposition increases congruity and promotes stability (Edmunds, 2011). This morphology allows the thumb to perform multiplanar motions such as abduction, adduction, circumduction, extension, flexion, reposition, and the critical function of opposition. In turn, these multiplanar movements permit key daily tasks such as pinch, grasp and jar twist (Edmunds, 2011).
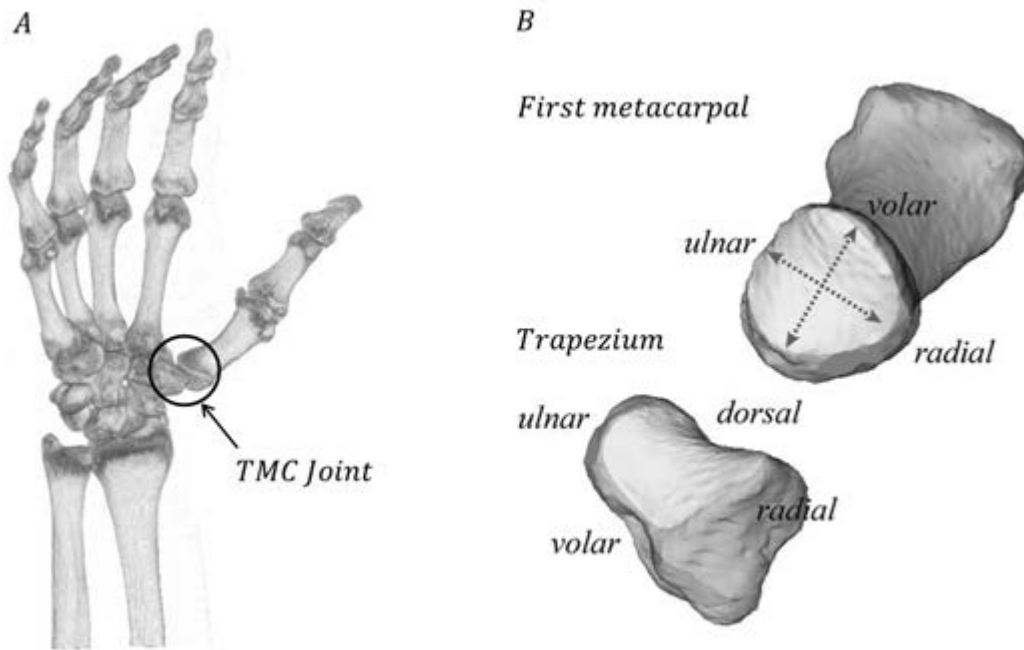
Figure 1.3. Location of the TMC joint in the right hand (A), and an exploded view of the TMC joint bones (B) showing the biconcavoconvex (saddle) morphology and joint axes. Adapted from Halilaj et al. (2014a).
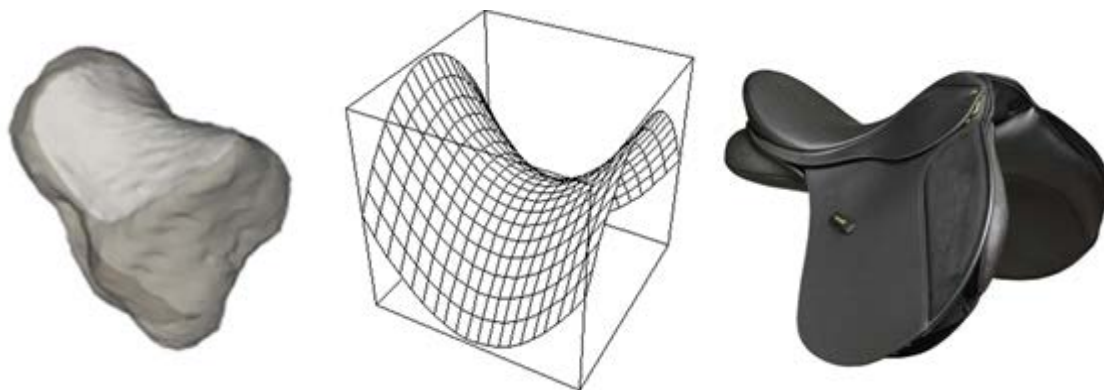
Figure 1.4. Saddle shape of the articular surface of the TMC joint surfaces permit multiplanar motions.

1.2.1 Ligaments

The wide range of mobility displayed by the TMC joint comes at the cost of reduced stability. The relative stability of the TMC joint is provided by the surrounding soft tissue, including: joint capsule, muscles, and ligaments. As many as 16 ligaments are thought to play a role in stabilising the joint (Bettinger et al., 1999, Van Brenk et al., 1998). For the purpose of this thesis we will introduce the main ligaments in the TMC joint: the dorsal ligament complex and the volar beak ligament.

The dorsal ligament complex – consisting of three sub-ligaments, including the dorsal radial, dorsal central, and posterior oblique sub-ligaments – is the most important ligament of the TMC joint. Also known as the dorsal deltoid ligament, it connects the dorsal base of the first metacarpal to the dorsal tubercle of the trapezium. The ligament has a mean thickness of 1.85 mm ± 0.14 mm, is consistently located in the same site, and possesses the highest strength, stiffness, and toughness of all ligaments in the TMC joint (Ladd et al., 2013). Together with the volar beak of the first metacarpal, the dorsal ligament complex stabilises the TMC joint by preventing the disengagement of the beak and the dorsal subluxation of the metacarpal base. When cut or torn as a result of trauma such as dislocation, the TMC joint is unable to achieve stability and will dislocate (Edmunds, 2011).

The volar beak ligament is described as a thin, weak, curtain-like structure covering the volar surface of the TMC joint (Edmunds, 2011, Pieron, 1973). Also known as the palmar beak ligament, volar anterior oblique ligament, ulnar ligament, and various other names, it extends from the volar beak of the first metacarpal and connects on the volar face of the trapezium. The ligament has a mean thickness of 0.71 mm, variable width, is inconsistently located in the TMC joint, consists of poorly organised connective tissue, and is lax in all positions apart from full extension (Halilaj et al., 2015c, Ladd et al., 2013).

When the volar beak ligament is cut, the TMC joint still functions without it and can stabilise with the screw home mechanism (Edmunds, 2011). This supports the hypothesis that the volar beak ligament is not truly a ligament, but instead a disorganised film of connective tissue (Ladd et al., 2013).
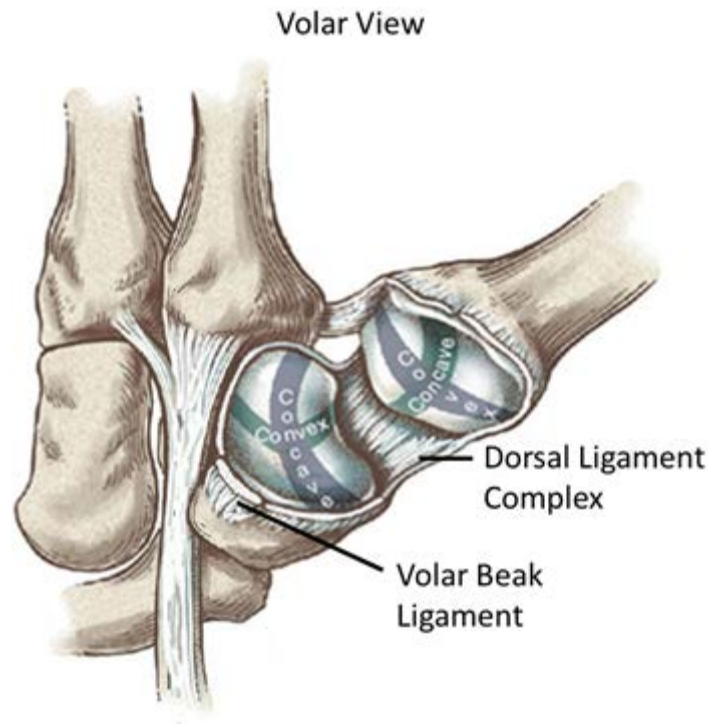
Figure 1.5. Volar view of a right thumb showing the main ligaments of the TMC joint: dorsal ligament complex and volar beak ligament. Adapted from Neumann (2013).

1.2.2 Muscles

Many of the ligaments are lax during the range of motion the TMC can perform (Halilaj et al., 2015c, Tan et al., 2011). The laxity of the joint throughout a large range of motion supports the notion that neuromuscular control of muscles is responsible for TMC joint stability. Muscles that are involved in dextrous manipulation of the thumb can be categorised into extrinsic and intrinsic muscles.

Extrinsic muscles have their muscle body located in the forearm and include: abductor pollicis longus, extensor pollicis longus, extensor pollicis brevis, flexor pollicis longus (Figure 1.6).

Intrinsic muscles are located entirely within the hand, and include those of the thenar eminence: abductor pollicis brevis, flexor pollicis brevis, opponens pollicis, and other intrinsic muscles such as the adductor pollicis and the first dorsal interosseous (Figure 1.6).
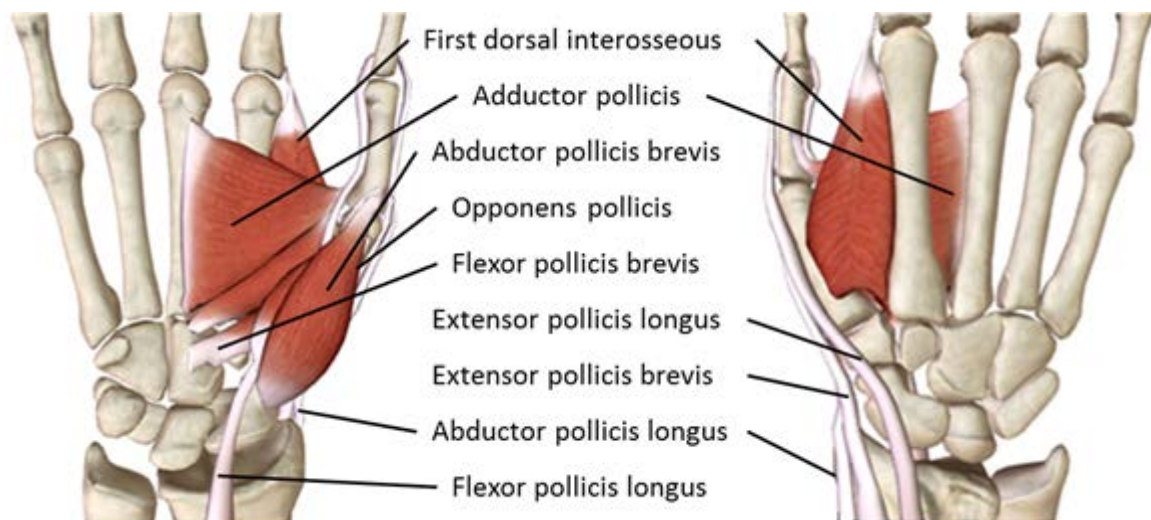
Figure 1.6. Intrinsic muscles and tendons of extrinsic muscles involved in TMC joint kinematics. Adapted from Qualter et al. (2011).

The abductor pollicis longus and abductor pollicis brevis muscles work together to perform abduction. Extensor pollicis longus and extensor pollicis brevis muscles work together to perform extension. Flexion is achieved by the flexor pollicis longus and the flexor pollicis brevis muscles. Adduction and opposition occurs through the contraction of the adductor pollicis and the opponens pollicis muscles (Figure 1.7). The first dorsal interosseous coordinates with the opponens pollicis muscle to stabilise the TMC joint (Gray, 1918).

The forces experienced in the TMC joint during tasks such as pinch and grasp originate from three sources: internal muscle forces, external forces, and passive

soft-tissue forces. Assuming no external forces, Cooney and Chao (1977) showed that TMC joint reaction forces during lateral pinch can be 12 times the force generated at the tip of the thumb, with shear stresses in the joint up to 2.5 times. During forceful grasp, the muscles can generate large compressive forces of up to 1.2 kN in the TMC joint (Cooney and Chao, 1977). Precise neuromuscular coordination of these muscles is important to maintain normal biomechanics, and provides stability for this mobile joint.
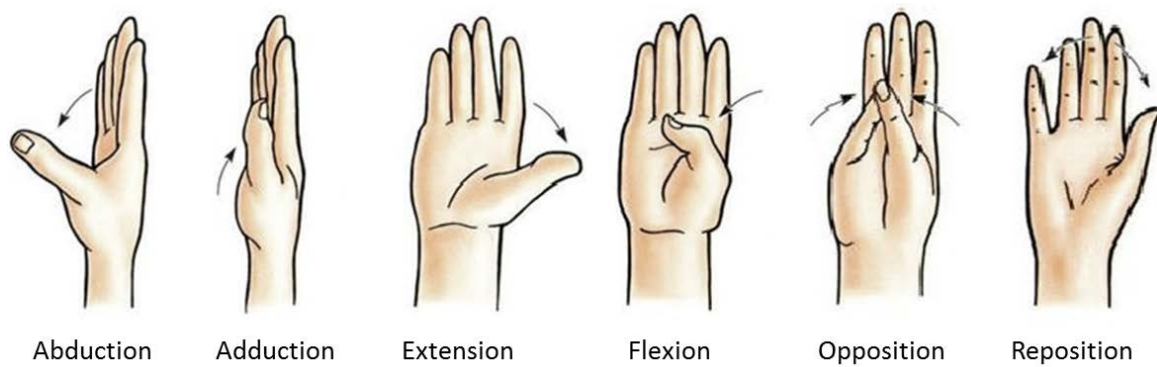
Figure 1.7. Motions of the thumb permitted by the TMC joint.

1.2.3 Cartilage

Articular cartilage is important to the function and health of the TMC joint. It is responsible for providing a smooth, lubricated surface to facilitate the dispersion of forces in the TMC joint with minimum friction in the joint. This is achieved through its unique structure: a dense extracellular matrix – mainly composed of water (75 % to 80 %), 5 % proteoglycans, and 15 % collagen fibres – that is sparsely distributed with cartilage cells, or chondrocytes, which maintain the cartilage and produce the extracellular matrix. The collagen fibres are aligned such that a multi-zonal structure results (Figure 1.8). In the superficial zone, the collagen fibres are aligned tangentially, allowing cartilage to resist large compressive forces by dispersion of the force. The middle zone constitutes up to 60 % of the cartilage volume, and has collagen fibres aligned

obliquely. In the deep zone these fibres become thicker and perpendicularly aligned to the articular surface, allowing great resistance to compressive forces. Finally, the calcified zone secures the cartilage to the subchondral bone.
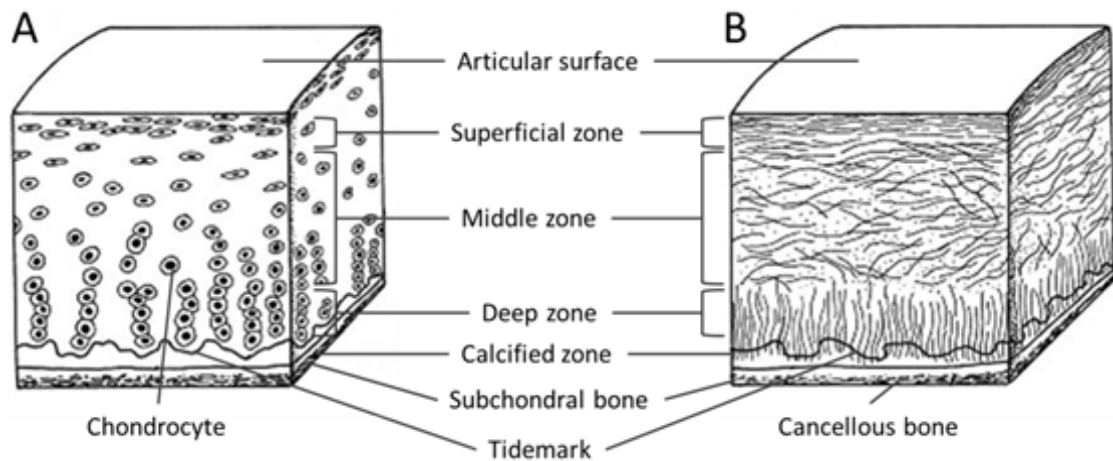
Figure 1.8. Cross-sectional diagram of healthy cartilage structure showing cellular organisation (A), and collagen fibre orientation (B). Adapted from Sophia Fox et al. (2009).

Cartilage responds to mechanical stress and strain throughout growth and development, injury, and degeneration. Water resides between hydrophilic proteoglycan fibres resulting in a viscoelastic biomechanical behaviour that can be considered to have biphasic properties: an incompressible fluid phase and a fibrous matrix phase. These phases allow cartilage to tolerate compressive hydrostatic stresses very well, as the fluid phase is able to support high pressures. However, the fibrous matrix fails when placed under high shear stresses or tensile strains (Carter et al., 2004). As such, ossification of cartilage has been shown to be inhibited by a cycle of intermittent hydrostatic compressive stress, which maintains the cartilage. However, intermittent octahedral shear stress can accelerate ossification by causing destructive tensile strain (Carter et al., 2004).

In the TMC joint, cartilage mechanics has been poorly documented and the morphology and mechanical properties are an area where more study is warranted. Cartilage mechanics in the TMC joint has been qualitatively described in clinical studies (North and Rutledge, 1983, Van Nortwick et al., 2013, Xu et al., 1998) but the thickness and material properties were not quantified. The thickness has been quantitatively described in early to late osteoarthritic cadaveric TMC joints using stereophotogrammetry (Koff et al., 2003). In their study, Koff et al. (2003) reported that the mean cartilage thickness was approximately uniform throughout the articular surface with a thickness of 0.8 mm in both the first metacarpal and trapezial bones of early osteoarthritic (Stage I) cadavers (Figure 1.9). These researchers also showed that cartilage became thinner and less uniform with the progression of OA (Figure 1.9). Therefore, we would expect healthy cartilage to exhibit similar properties to those that exhibited early OA. However, along with mechanical testing of TMC joint cartilage properties, this work has not been completed and is an area that requires further investigation.
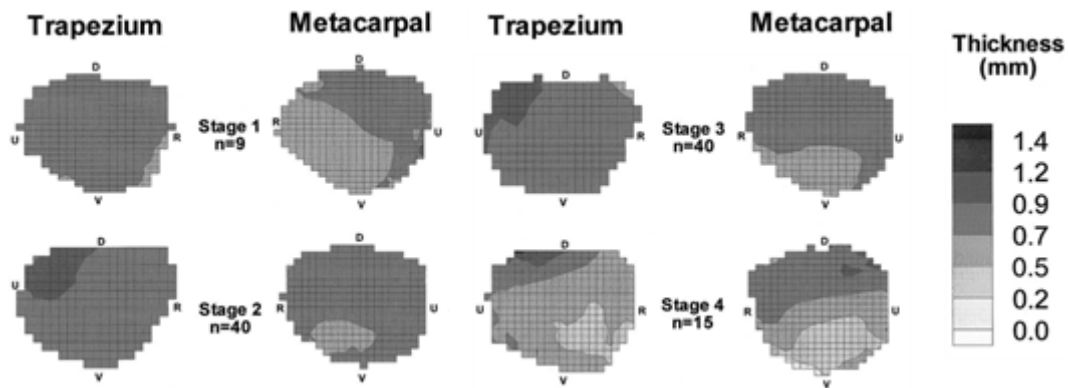
Figure 1.9. Cartilage thickness maps in TMC cartilage with OA. Adapted from Koff et al. (2003).

Although cartilage displays biphasic properties, Ateshian et al. (2007) showed that the instantaneous response of a neo-Hookean hyperelastic material is

equivalent to that of a biphasic material subjected to fast loading, due to minimal fluid flow during fast loading conditions (Ferguson et al., 2003, Macirowski et al., 1994). Many studies have modelled cartilage as a linear-elastic material (Anderson et al., 2007, Butz et al., 2011, Hadid et al., 2012), or neo-Hookean hyperelastic material (Anderson et al., 2008, Anderson et al., 2010, Büchler et al., 2002, Butz et al., 2011) with results that are comparable to those obtained experimentally. Biphasic material models are used to quantify the fluid flow within the joint when studying the effects of creep and stress relaxation. True cartilage exhibits anisotropic variation in material properties across its surface, and throughout its depth, as well as tension-compression nonlinearity. For the purpose of this thesis, characterising stress distributions and determining contact areas can be sufficiently done by modelling cartilage as a neo-Hookean material.

1.3   TMC joint OA

The TMC joint is a common site of degenerative OA. TMC joint OA is widespread, affecting 15 % of adults over the age of 30, and two to six times more women than men (Dias et al., 2007, Haara et al., 2004, Valdes and von der Heyde, 2012). Armstrong et al. (1994) reported that 1 in 4 women and 1 in 12 men will eventually have radiological signs of TMC OA. Despite being the second most common site of OA in the hand, it is has the highest incidence of surgery due to its significant effect on disability. The symptoms of early OA include mild pain, instability, subluxation, joint space narrowing, and decreased range of movement (Batra and Kanvinde, 2007). Later stage symptoms include deformity, eburnation, osteophytic growths, severe pain, and complete loss of motion (Batra and Kanvinde, 2007, Najima et al., 1997). Because object handling and grasping is only possible with the critical function of opposition, TMC OA can impair the upper extremity by up to 50 % (Pellegrini Jr, 2005).

The aetiology of TMC OA onset is poorly understood. Although many risk factors have been identified – including sex, obesity, occupational risk factors, hereditary factors, hormonal, and joint laxity – the mechanism and events that result in the onset of OA have yet to be delineated. Several factors are implicated in the pathogenesis, with consensus that biomechanical factors are paramount (Hunter et al., 2005). The main hypotheses in the literature (Najima et al., 1997) include ligament laxity due to hormonal change or trauma (Pellegrini, 1991), hypoplasia of the trapezial joint surface (North and Rutledge, 1983), abnormality in abductor pollicis longus (Brunelli and Brunelli, 1991), imbalance between adductor pollicis and abductor pollicis longus (Brunelli and Brunelli, 1991), joint incongruence (Eaton and Littler, 1973), and synovial inflammation (Dingle, 1981). Many of these hypotheses point towards abnormal or repetitive loading of TMC cartilage, resulting in cartilage wear and growth of osteophytes.

1.4 Previous literature on TMC joint function

Over the last half-century, our understanding of TMC joint anatomy, function, and disease, has progressed due to a combination of biomechanics research, clinical research, and epidemiology. The general consensus is that osteoarthritic degeneration is the result of biomechanical response to abnormal cartilage stresses and strains. The factors that play a role in determining the stresses and strains experienced in the cartilage are: morphology, kinematics (e.g. task or posture), forces (internal and external forces), and material properties (e.g. Youngs modulus of bone and cartilage).

Much of the prior work has been dedicated to describing the morphology of the TMC joint, in particular the curvatures and congruence of the articular surface (Ateshian et al., 1992, Conconi et al., 2014, Halilaj et al., 2014b, Kovler et al., 2004, North and Rutledge, 1983, Van Nortwick et al., 2013, Xu et al.,

1998). These studies have used a range of methods including simple descriptive classification (Van Nortwick et al., 2013), dial indicator measurement of curvature (North and Rutledge, 1983), mathematical modelling of curvature through stereophotogrammetry of cadavers (Ateshian et al., 1992, Xu et al., 1998), clinical computed tomography (CT) of osteoarthritic patients (Conconi et al., 2014, Halilaj et al., 2014b), and laser scanning (Kovler et al., 2004) to investigate the articular surface morphology. There is some disagreement between studies regarding shape differences between TMC joints of men and women. Recent CT imaging-based studies have determined that there are no sex differences in the articular shape of the TMC joint by studying articular surface congruence (Conconi et al., 2014, Halilaj et al., 2014b). Congruence is an important factor that is dependent on joint orientation and directly influences the stress and strain implicated at the pathogenesis of OA. However, stress and strain are dependent on contact specific congruence, and factors such as the kinematics, forces, and contact posture, which have not been considered. Furthermore, the morphology of the entire TMC joint bones and the length of the muscle moment arms during contact can influence the stress and strain experienced in the cartilage. Ideally, an analysis of morphology should be made using a correspondent (parametric) model such that shape parameters are compared in the same frame of reference. This would also allow the *in silico* analysis of contact, stress, and strain to be comparable across tasks and genders.

Another large section of work in this field is dedicated to the kinematics. Halilaj et al. (2014d) reported that TMC joint kinematics appear to be influenced by age, but not sex. This difference is thought to be a result of degenerative morphological changes. The same group has characterised the complex envelope of motion in the healthy TMC joint (Crisco et al., 2015b). Kinematics is an important factor that is responsible for the posture of the joint during contact. Reports of contact location in the TMC joint have been contradictory.

Contact areas have been reported on the dorsal side (Eaton and Littler, 1969), volar-ulnar quadrant (Ateshian et al., 1995), as well as the volar-radial quadrant (Halilaj et al., 2015b, Kuczynski, 1974, Napier, 1955, Pieron, 1973). Most studies have been performed *in vitro* using cadaver hands and were unable to incorporate realistic kinematics. This analysis could also be performed *in silico* using CT imaging based computational models, such as the joint space centroid calculation (Halilaj et al., 2015b). We propose to use population based contact models across a range of tasks to gain insight into the stress and strain distribution in the cartilage. The estimation of *in silico* muscle forces must also be made, and remains a significant challenge.

A few studies have attempted to calculate the forces in the TMC joint during various tasks (Cooney and Chao, 1977, de Monsabert et al., 2014, Giurintano et al., 1995, Valero-Cuevas et al., 2003, Wohlman and Murray, 2013). Cooney and Chao (1977) showed that forces in the TMC joint could be as high as 12 times the force generated at the tip of the thumb during lateral pinch. During forceful grasp, muscles were able to generate compressive forces of up to 1.2 kN. Ligament disruption studies indicate that the volar-beak ligament doesn't play a role in tasks such as grasping and pinching, rather that stability is achieved through neuromuscular control and the screw-home mechanism. Wohlman and Murray (2013) created a model that produced end-tip forces of the index finger. However, these studies do not report individual forces for the muscles involved in producing TMC motion. Furthermore, they do not investigate the stress and strain experienced in the TMC joint cartilage or investigate sex differences.

To the author's knowledge, TMC joint cartilage properties have only been briefly examined by Rivers et al. (2000) in a study that examined aggregate modulus and biochemical composition in a cohort of 53 cadavers with normal to advanced TMC OA. TMC joint cartilage properties such as Young's modulus and morphology remain an area for future investigation.

1.5   Objectives

The aim of this work was to create a computational framework to investigate the relationship between TMC morphology, kinematics, and cartilage stress distributions in men and women with and without degenerative disease. This aim was achieved by addressing the following objectives:

1. Develop a statistical shape model (SSM) of the TMC joint bones;

2. Develop a SSM based automatic segmentation tool;

3. Characterise the healthy three-dimensional morphology of the TMC joint bones as a function of sex and age;

4. Develop a parametric population based finite element (FE) model of the TMC joint;

5. Estimate the cartilage stress distributions of the TMC joint throughout a range of motion;

6. Classify the cartilage stress distributions, contact area, and peak stress location, as a function of sex, age, and task;

7. Develop a SSM based classifier of the TMC joint bones;

8. Characterise the shape differences between healthy and early osteoarthritic TMC joints;

9. Evaluate the efficacy of using linear discriminant analysis (LDA) based SSM as a clinical tool for detecting early stage OA.

1.6 Thesis overview

This thesis is organised into the following sections:

- Chapter 2 presents an automatic segmentation pipeline of the thumb TMC joint using parametric statistical shape modelling and random forest regression voting (objective 2);

- Chapter 3 presents a SSM of the healthy TMC joint (objective 1) and investigates the relationships between sex, age, and morphology (objective 3);

- Chapter 4 specifies a population based FE model (objective 4) for simulating mechanics and inferring cartilage stress distributions (objective 5) to investigate the differences in TMC joint contact as a function of sex and age during three isometric functional tasks (objective 6);

- Chapter 5 demonstrates the use of a SSM based classifier (objective 7) for characterising shape differences between healthy and early osteoarthritic TMC joints (objective 8) and discusses the use of such a tool for automatically detecting early OA in the clinic (objective 9);

- Chapter 6 outlines the key findings of this thesis, the contributions to the literature, the limitations of the thesis, and the future directions for this work.

1.7 Novel contributions

This thesis contributes to the fields of clinical biomechanics and musculoskeletal modelling. It applies image analysis, statistical modelling, FE modelling, machine learning, and numerical optimisation techniques to investigate the biomechanics of TMC joint OA. Specifically, the novel contributions are:

- Development of the first SSM of healthy TMC joint bones and corresponding quantification of morphology in a population of 50 healthy subjects;

- Development of the first random forest regression voting (RFRV) and SSM based automatic segmentation tool for the TMC joint;

- Development of the first parametric population force-driven FE model of the TMC joint;

- *In silico* calculation of normalised TMC joint stress distributions, contact areas, and location of peak stresses for three tasks;

- Development of the first LDA classifier based on a SSM of 50 healthy and 75 early osteoarthritic TMC joint bones, and corresponding quantification of morphologic differences between TMC joints that are healthy and those that exhibit early OA.

1.8 Research outputs

This thesis has been presented through the following collected works:

Journal publications

- Schneider, M., Zhang, J., Crisco, J., Weiss, A., Ladd, A., Nielsen, P. & Besier, T. 2015. Men and women have similarly shaped carpometacarpal joint bones. *Journal of biomechanics*, 48, 3420-3426.

- Schneider M., Zhang J., Crisco J., Weiss A., Ladd A., Mithraratne K., Nielsen P., Besier T. Accepted. Trapeziometacarpal joint contact varies between men and women during three isometric functional tasks. *Medical Engineering and Physics.*

- Schneider M., Zhang J., Crisco J., Weiss A., Ladd A., Nielsen P., Besier T. In Review. Early morphologic changes in trapeziometacarpal joint bones with osteoarthritis. *Osteoarthritis and Cartilage.*

- Schneider M., Zhang J., Crisco J., Weiss A., Ladd A., Nielsen P., Besier T. In Review. Automatic segmentation of the thumb trapeziometacarpal joint using parametric statistical shape modelling and random forest regression voting. *Computer Methods in Biomechanics and Biomedical Engineering: Imaging & Visualization.*

Encyclopaedia publication

The work in Chapter 3 has contributed to an article in a new dynamic encyclopaedia by Elsevier.

- Fernandez, J., Yeung, S., Swee, A., Schneider, M., Besier, T., Zhang, J. Accepted. On the use of population-based statistical models in biomechanics. *Encyclopedia of Biomedical Engineering.*

Conference papers and extended abstracts

- Schneider, M., Zhang, J., Crisco, J., Weiss, A., Ladd, A., Nielsen, P., & Besier, T. 2017. Early morphologic changes in trapeziometacarpal joint bones with osteoarthritis. *Poster presented at the Auckland Bioengineering Institute research forum*, February, Auckland, New Zealand.

- Schneider, M., Zhang, J., Crisco, J., Weiss, A., Ladd, A., Nielsen, P., & Besier, T. 2016. Statistical shape modelling detects subtle morphological differences in TMC joint morphology between healthy and early osteoarthritic subjects. In S. McGlashan (Chair). *Paper presented at the 8th Annual Mechanobiology Symposium*, November, Auckland, New Zealand.

- Schneider, M., Zhang, J., Crisco, J., Weiss, A., Ladd, A., Nielsen, P., & Besier, T. 2015. An automated pipeline for analysing contact stresses in the carpometacarpal joint. *Poster presented at the meeting of the Australian & New Zealand Orthopaedic Research Society*, October, Auckland, New Zealand.

- Schneider, M., Zhang, J., Crisco, J., Weiss, A., Ladd, A., Nielsen, P., & Besier, T. 2015. Women have similar carpometacarpal joint morphology to men. *Paper presented at the meeting of the Hand and Wrist Biomechanics International Symposium*, June, Milan, Italy.

- Schneider, M., Zhang, J., Crisco, J., Weiss, A., Ladd, A., Nielsen, P., & Besier, T. 2015. Automatic segmentation of the thumb carpometacarpal joint. *Poster presented at the Auckland Bioengineering Institute research forum*, February, Auckland, New Zealand.

- Schneider, M., Zhang, J., Crisco, J., Weiss, A., Ladd, A., Nielsen, P., & Besier, T. 2014. Automatic segmentation of the thumb carpometacarpal joint. *Poster presented at the meeting of the World Congress of Biomechanics*, August, Boston, MA.

- Schneider, M., Zhang, J., Crisco, J., Weiss, A., Ladd, A., Nielsen, P., & Besier, T. 2014. A statistical shape model of the thumb carpometacarpal joint. *Poster presented at the Auckland Bioengineering Institute research forum*, February, Auckland, New Zealand.

- Schneider, M., Zhang, J., Crisco, J., Weiss, A., Ladd, A., Nielsen, P., & Besier, T. 2013. A statistical shape model of the thumb carpometacarpal joint. *Paper presented at the meeting of the International Thumb Osteoarthritis Workshop*, October, Newport, RI.

Chapter 2.

Automatic segmentation of the thumb trapeziometacarpal joint using parametric statistical shape modelling and random forest regression voting

The following is a reproduction of the article (In review):

2.1 Abstract

Existing segmentation algorithms including manual, semi-automatic, and automatic segmentations methods for acquiring anatomically accurate 3D bone models are unsuitable for incorporation into automatic pipelines and batch processes due to their time-consumption, requirement for manual input, and requirement for mesh post-processing before further analysis can be carried out. We propose an automatic pipeline for creating shape modelling suitable

parametric meshes of the TMC joint from clinical CT images for the purpose of batch processing and analysis. The method uses 3D RFRV with SSM segmentation. For each mesh node, random forest (RF) regressors are trained with the omni-directional distribution of displacements of expected image features (3D Haar-like features) around the node. During segmentation of a new image, 3D Haar-like features are randomly sampled in an omni-directional search space for each RF regressor, resulting in a map of votes for the predicted location of the desired object. The mesh is then fitted to the predicted nodes via deformations permitted by the SSM. The method was demonstrated in a validation experiment involving 65 CT images, 15 of which were randomly selected to be excluded from the training set for testing. With mean root mean squared (RMS) errors of 1.066 mm and 0.632 mm for the first metacarpal and trapezial bones respectively, and a segmentation time of ~2 minutes per CT image, the preliminary results showed promise for providing accurate 3D meshes of TMC joint bones for batch processing.

2.2 Introduction

The TMC joint is highly susceptible to OA, and can impair the upper extremity by up to 50 % (Pellegrini Jr, 2005). Several factors have been implicated in its pathogenesis, with biomechanical factors paramount (Hunter et al., 2005). Morphology of the first metacarpal and trapezial bones are important biomechanical factors that must be considered as they affect the moment arms of muscles and ligaments, joint kinematics, posture during tasks, and the cartilage stresses and strains during contact(Arnold and Delp, 2001, Halilaj et al., 2014b, Nanno et al., 2006).

Anatomically accurate 3D models of the TMC joint can be obtained through segmentation of clinical CT volumes. However, traditional manual and semi-automatic segmentation methods are time-consuming and require manual

intervention to complete the segmentation of an image volume. The segmented data, usually in the form of point clouds, require meshing or triangularisation prior to musculoskeletal modelling, FE analysis, or shape modelling. Therefore, these methods are unsuitable in workflows that involve batch processing, where the speed of segmentation is important, minimal user input is desired, and data may be required in certain formats for further processing.

Automatic segmentation methods address the main disadvantages of both manual and semi-automatic methods by removing the requirement of manual intervention; they are time efficient, and can be used in batch processes. This would allow for a potential clinical tool such as an automated pipeline that processes CT volumes for useful information such as the corresponding stress distributions. However, automatic segmentation methods such as region growing, active shape models (ASM), point distribution model based SSM segmentation methods, may suffer from decreased robustness because of their reliance on correct initialisation, linear search spaces perpendicular to the model surface, high contrast edges, and high resolution relative to object feature size. In the wrist, these automatic segmentation methods struggle with the crowding of carpal bones and small joint spaces relative to voxel dimensions that create low contrast edges, especially in lower resolution clinical CT.

Three-dimensional RFRV automatic shape model segmentation uses randomly sampled image features (e.g. 3D Haar-like features) to train a forest of decision trees to predict the most likely image location of the desired model. This has been demonstrated in 2D with facial recognition (Cootes et al., 2012) and 2D segmentation of the proximal femur (Lindner et al., 2013), and more recently demonstrated in 3D in the Liver (Norajitra et al., 2015). This method can be combined with parametric statistical shape modelling to create an automatic segmentation pipeline that has increased robustness to initialisation, increased speed of segmentation, and automatic meshing for downstream analysis.

The purpose of this chapter is to present a pipeline for automatically creating parametric meshes of the TMC joint from clinical CT images for the purpose of batch processing, shape modelling, and analysis. We detail the pipeline below then present quantitative segmentation results on a set of 65 clinical CT images of the wrist.

2.3 Methods

The method uses a SSM combined with RFRV to perform automatic segmentation of the TMC joint. A SSM is first created and trained with segmented point clouds. RF regressors are trained on CT image data for each node. During segmentation, RF regressors predict the location of nodes in new CT images and the SSM is fit to the predicted nodes (Figure 2.1).
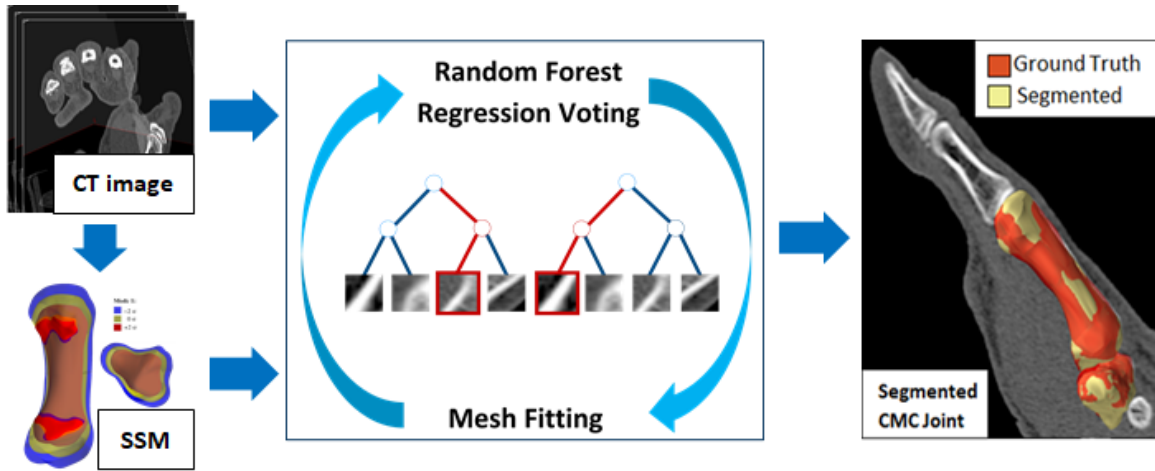
Figure 2.1.Automatic segmentation pipeline.

2.3.1 Statistical shape model

A parametric shape model is required to train the RF regressors, constrain the possible segmentation geometries, and to yield a parametric mesh of the desired geometry.

The parametric SSM is generated using a published method (Schneider et al., 2015) that is based on techniques described by Zhang et al. (2014). In summary, this method uses a custom template mesh consisting of cubic Lagrange elements (Nielsen, 1987) to represent the morphology. The mesh is designed to capture the morphological variation in anatomical landmark regions across the population. The template mesh is then fit to all point clouds in the training set through an iterative fitting process involving a series of coarse and fine fits. The fitted meshes of the training set are then rigidly aligned by minimising the squared distances of corresponding nodes. Principal component analysis (PCA) (section 2.3.2) is performed on the mesh nodal coordinates to produce an initial shape model. This process is repeated by using the shape model instead of the template mesh, until the RMS error is less than the in-plane pixel resolution. Thus, fitting correspondence is propagated and the meshes are maximally correspondent (Zhang et al., 2014). The final shape model is produced by performing a final PCA on the nodal coordinates of the maximally correspondent training set meshes.

2.3.2 Principal component analysis

Principal component analysis is performed to remove linear dependencies and for dimensionality reduction and allows any shape, x, in the training set to be reconstructed by the weighted sum of n principal components, ϕ, and the mean shape, $\bar{x}$ (Heimann and Meinzer, 2009, Schneider et al., 2015, Zhang et al., 2014):

$$x = \bar{x} + \sum_{i=0}^{n} \omega_i \phi_i \tag{2.1}$$

2.3.3 Random forest regression voting

Segmentation can be achieved by automatically locating the position of each mesh node in the CT image. This detection is performed by a RF regressor trained for each node.

For each regressor, 3D Haar-like features (section 2.3.4) are randomly sampled about the corresponding mesh node in an omni-directional search space. The regressors learn the spatial distribution of the 3D Haar-like features by associating the features with the displacement vector that points to the node position (Figure 2.2). When features are sampled from an unseen image, the regressors can predict its displacements based on the value of the 3D Haar-like features sampled, allowing for prediction of nodal locations.
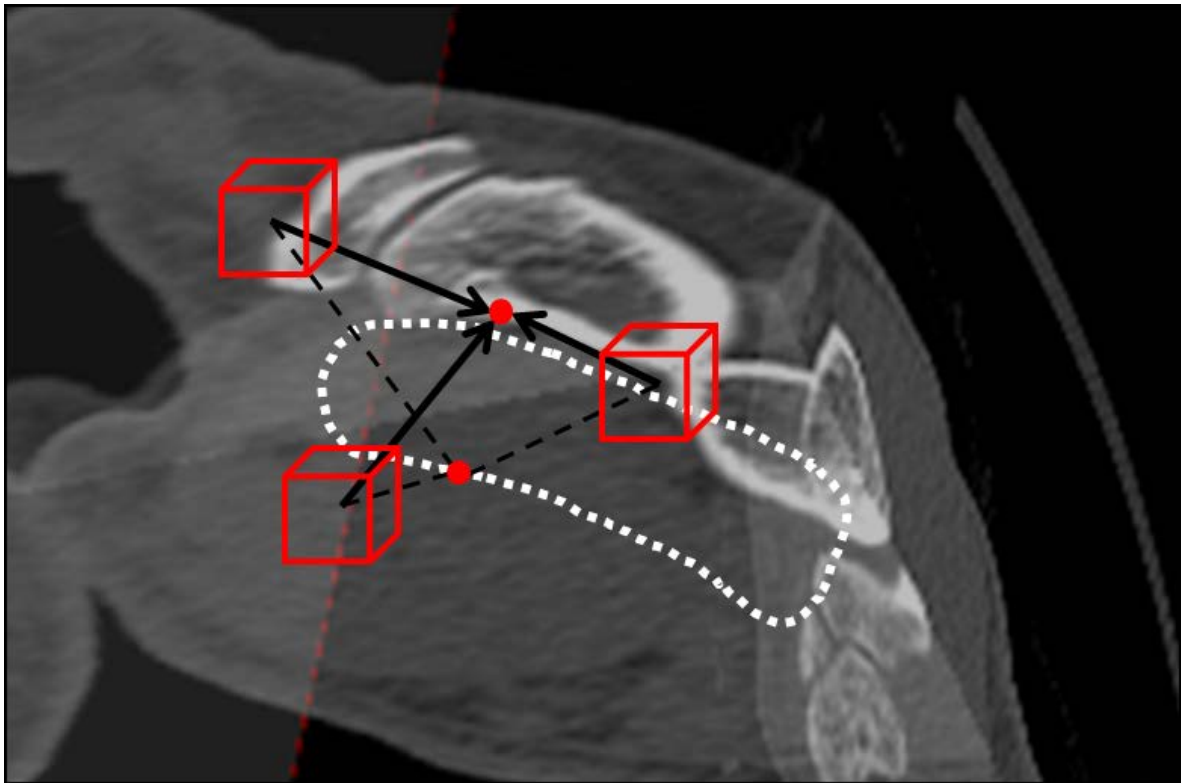
Figure 2.2. 3D Haar-like features (red boxes) and corresponding displacements (arrows) are used to train a RF regressor on the spatial distribution of features around each node of the shape model mesh. During segmentation, the shape model mesh (white dotted line) is initialised and 3D Haar-like features (red boxes) are sampled (dashed lines) from the mesh node (red point on white dotted line). The regressor for each node uses the features to predict the correct location (arrow) of the node (red point) in the CT image.

During segmentation, the mean mesh of the SSM is initialised, ideally in a neighbourhood of the desired object. Each tree in the RF regressor of each node votes by estimating the displacement vector that points to the location of the mesh node from the sampled 3D Haar-like feature. This creates a distribution of votes that predict the location of the node in the CT volume. The mean location of the votes is taken as the final prediction of the best-matched image location of the mesh node. This process is performed for each node in each mesh to obtain the predicted nodal locations of the desired image geometry. The mean mesh is then fit to the predicted nodal locations using deformations permitted by the SSM (Equation 2.1), resulting in a segmented mesh. Meshes segmented with this shape model are also parametric, allowing subsequent analysis of morphology and stress analysis to be directly compared in the same frame of reference.

2.3.4 3D Haar-like features

Haar-like features are used in image object recognition and have been used in image segmentation in 2D (Cootes et al., 2012) and 3D (Norajitra et al., 2015). Haar-like features are calculated by comparing the difference in summed pixel intensity between adjacent regions of pixels (in 2D) or voxels (in 3D) within a bounding box (Figure 2.3). These features can be calculated efficiently by precomputing the integral image using the equation 2.2:

$$I_{\Sigma(x,y,z)} = \sum_{\substack{x' \le x \\ y' \le y \\ z' \le z}} i(x', y', z')$$

$$(2.2)$$
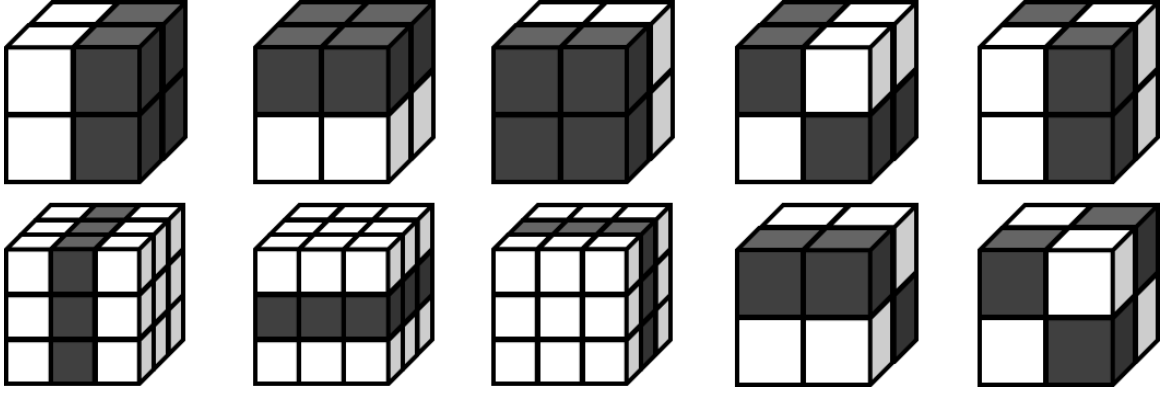
Figure 2.3. The ten types of 3D Haar-like features that were used to train the RF regressors. Feature values were calculated by comparing the difference in summed pixel intensities in the dark and light bounding boxes.

2.4 Validation experiment

The method described above was applied to a set of 65 clinical CT images from healthy adult males and females. The wrist was imaged in clinical neutral position with a 16-slice clinical CT scanner (GE LightSpeed 16, General Electric, Milwaukee, WI). The scanner was set with the following settings: tube voltage at 80 kVp, tube current at 80 mA, slice thickness of 0.625 mm, and in-plane resolution of 0.4 mm ✕ 0.4 mm. The trapezia and first metacarpals were segmented semi-automatically using Mimics v12.11, and exported as triangulated surfaces. The vertices of the triangulated surfaces were extracted to obtain a training set of point clouds for the SSM.

Fifty CT images were randomly selected to be the training data set for the SSM and the RF regressors, and the remaining 15 CT images were used to evaluate the accuracy and performance of the method. Through leave-one-out analysis we found that 50 datasets produced a stable SSM and was sufficient to recover the important components that were used to comprehend and summarise multivariate data. A parametric template mesh was created for the first metacarpal, consisting of 398 nodes and 97 cubic Lagrange elements, and trapezium, consisting of 344 nodes and 52 cubic Lagrange elements. This

template mesh was used to create the SSM, consisting of 742 nodes, for the entire joint. 50 CT sampling windows, with a size of $10 \times 10 \times 10$ voxels, were randomly sampled within an omnidirectional search space of 30 voxels about each node in the CT image. Integral images were computed, and 3D Haar-like features were calculated and used to train the RF regressors that consisted of 20 random decision trees. The time required to train 742 RF regressors took approximately 3 hours on an Intel Xeon quad core computer.

To evaluate the accuracy and performance of the method, we applied the trained RF regressors to the remaining 15 CT images not used in training. The SSM was initialised in the centre of the CT images, near the in-image TMC joint bones. The RF regressors then predicted the locations of all 742 mesh nodes. The mesh was fit to the predicted node locations with the weighted sum of principal components; by minimising the least squared error between the predicted nodal coordinates and shape model node coordinates, producing a segmented parametric mesh of the TMC joint bones.

2.5 Results

The segmentation time for all 15 datasets was approximately 30 minutes on an Intel Xeon quad core computer. The average surface-to-surface RMS error between automatically segmented mesh and manually segmented ground truth for all 15 datasets was 1.066 mm in the first metacarpal and 0.632 mm in the trapezium (Table 2.1).

Table 2.1. Calculated error distributions (in mm) for test population (n = 15).

	Mean Error	RMS Error	Max Error	Min Error	Mean % Volume Overlap
1st Metacarpal	0.997 ± 0.372	1.066	2.110	0.0457	84.12 %
Trapezium	0.564 ± 0.282	0.632	1.776	0.013	86.03 %

Figure 2.4 shows the mean pointwise error distribution of all 15 datasets. The largest errors appear to occur in regions of high curvature. Figure 2.5 shows the segmentation of a randomly selected dataset overlapped with the ground truth.
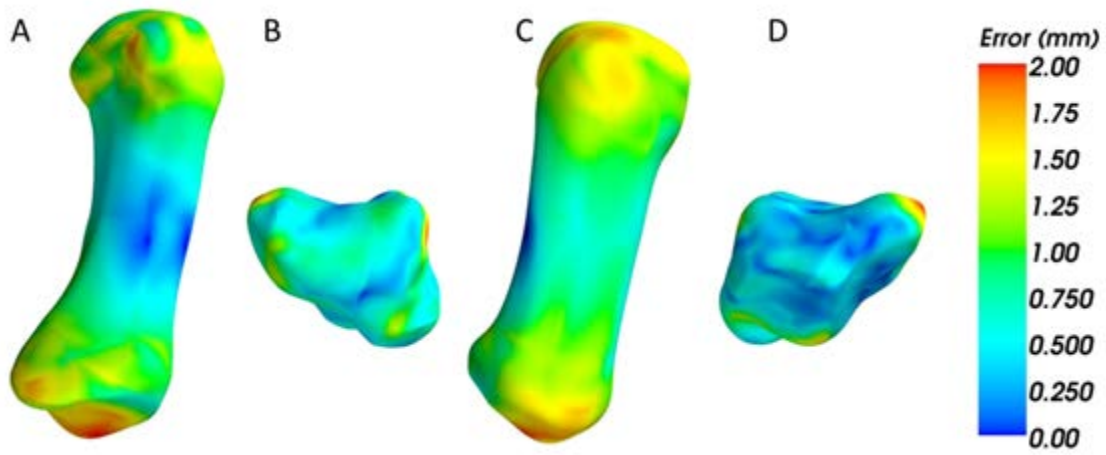
Figure 2.4. Mean pointwise error distribution plotted on an automatically segmented TMC. The volar-radial view (A), and dorsal view (C) are shown for the first metacarpal. The volar view (B) and dorsal view (D) are shown for the trapezium.
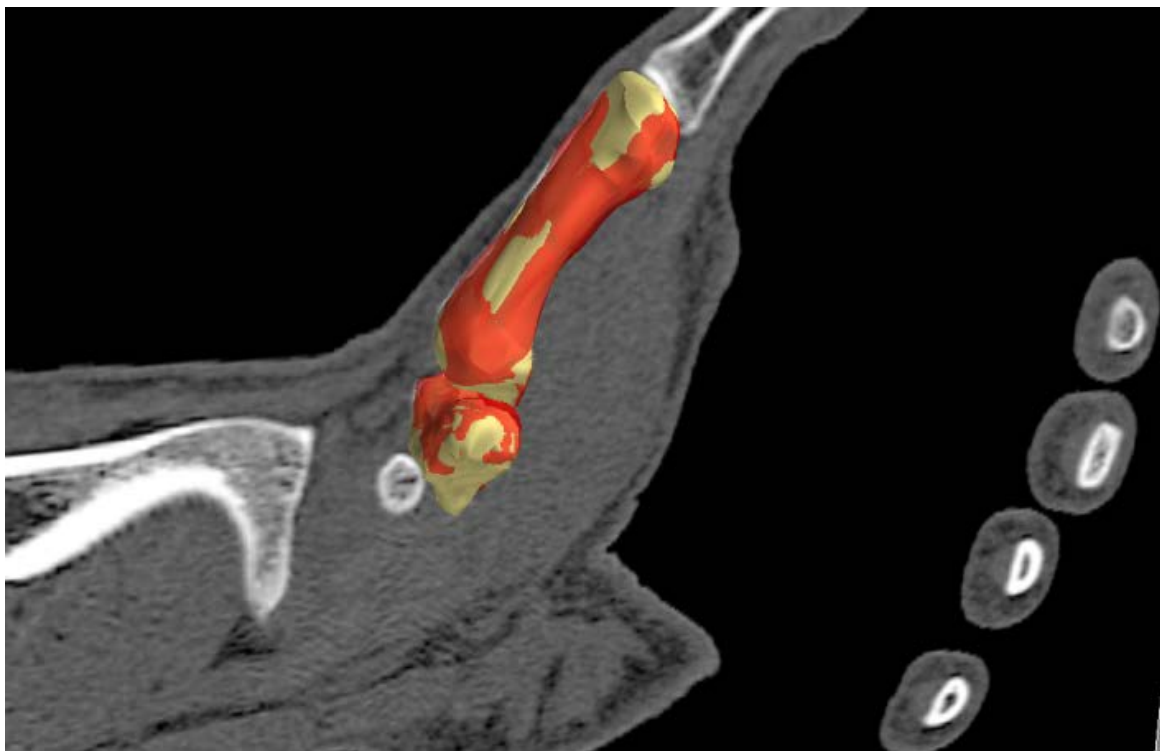
Figure 2.5. Segmented TMC joint bones. Red shows ground truth. Yellow shows automatically segmented mesh.

2.6 Discussion

These results show promise for a fully automatic segmentation pipeline that creates anatomically accurate parametric meshes from CT image data. Since the deformation of the mesh geometry was restricted by the SSM, the segmented shapes of the bones were constrained to be anatomically accurate. Pointwise error distribution plots of the automatically segmented surface compared with the manually segmented ground truth indicated that the error was highest about regions of high curvature (Figure 2.4). The mean error in the first metacarpal was $0.997\,mm \pm 0.372\,mm$, and $0.564\,mm \pm 0.282\,mm$ in the trapezium, which may be considered reasonable depending on the purpose of the model. The mean % volume overlap was 84.12 % in the first metacarpal and 86.03 % in the trapezium, is comparable to the volume overlap scores reported by Norajitra et al. (2015) on the liver, except in a much smaller joint. However, for the purpose of contact biomechanics at the articular surfaces of the joint, these errors may require further reduction, as the maximum errors (2.110 mm in the first metacarpal and 1.776 mm in the trapezium) are comparable to the size of the joint space in the TMC joint (~ 2 mm).

This pipeline appears to be robust to variation in the location of initialisation of the shape model. The success of ASMs and region growing algorithms are highly dependent on correct initialisation. In our test scenarios, as the TMC joint bones were the subject of interest, we assumed that the in-image position of the TMC joint bones would be close to the centre, and thus, it seemed reasonable to initialise the shape model in the centre of the CT images. However, the TMC joint was not perfectly located in the centre in any of the datasets, and was located up to 30 mm away. Despite this, the pipeline managed to segment the TMC joint bones to RMS errors of 1.066 mm in the first metacarpal and 0.632 mm in the trapezium. We expect that these errors can be improved by using a multi stage process. First, RF regressors trained with large windows and distances can be used to initialise the mesh closer to the joint.

Afterwards, incremental improvements in segmentation can be attempted by using RF regressors trained on smaller windows and distances. As the pipeline performs quickly (~2 minutes per segmentation) this step can be repeated a number of times to increase the accuracy of segmentation without sacrificing too much time. Segmentation accuracy could also be improved by increasing the training data set for both the statistical shape model and the random forest regressor.

2.7 Conclusion

We have presented a pipeline for automatically creating parametric meshes of the TMC joint from CT images of the wrist, using RFRV combined with parametric statistical shape modelling. This method has demonstrated increased flexibility in terms of segmentation error with regards to the location of initialisation compared to methods such as active shape modelling and region growing. The use of 3D Haar-like features were used to teach the spatial characteristics of the images to the RF regressors, and to predict the location of mesh nodes in new images. Our results were promising, with mean RMS errors of 1.066 mm and 0.632 mm for the first metacarpal and trapezial bones respectively. We propose a multistage process involving a series of coarse to fine segmentations to improve the segmentation accuracy. This pipeline has the potential to be used for rapid segmentation of clinical CT images, for the purpose of implant design, biomechanics analysis, and in surgical planning.

Chapter 3.

Men and women have similarly shaped carpometacarpal joint bones

The following is a reproduction of the article:

Schneider M, Zhang J, Crisco J, Weiss A, Ladd A, Nielsen P, Besier T. 2015. Men and women have similarly shaped carpometacarpal joint bones. *Journal of biomechanics*.48:3420-3426.

3.1 Abstract

Characterising the morphology of the TMC joint bones and how they vary across the population is important for understanding the functional anatomy and pathology of the thumb. The purpose of this chapter was to develop a SSM of the trapezial and first metacarpal bones to characterise the size and shape of the whole bones across a cohort of 50. We used this shape model to investigate the effects of sex and age on the size and shape of the TMC joint bones and the articulating surface area of the TMC joint. We hypothesised that women have similar shape trapezial and first metacarpal bones compared to men, following scaling for overall size. We also hypothesised that age would be a significant

predictor variable for TMC joint bone changes. CT image data and segmented point clouds of 50 TMC bones from healthy adult men and women were obtained from an ongoing study and used to generate two SSMs. Statistical analysis of the principal component weights of both models was performed to investigate morphological sex and age differences. We observed sex differences, but were unable to detect any age differences. Between men and women the only difference in morphology of the trapezia and first metacarpal bones was size. These findings confirm our first hypothesis, and suggest that the women have similarly shaped trapezial and first metacarpal bones compared to men. Furthermore, our results reject our second hypothesis, indicating that age is a poor predictor of TMC joint morphology.

3.2 Introduction

Characterising the morphology of the TMC joint bones and how they vary across the population is important for understanding the functional anatomy and pathology of the thumb. Bone size and morphology influences the articulating contact area and shape of the joint (Halilaj et al., 2014b), the location and action of ligaments (Nanno et al., 2006), and the kinematics, moment arms, and lines of action of muscles crossing the joint (Arnold and Delp, 2001, Hollister et al., 1992). These factors are critical for estimating the forces and stresses placed on the joint tissues (Anderson et al., 2010, Van Nortwick et al., 2013, Xu et al., 1998), which are important considerations for surgical implant design and believed to play a role in the mechanical aetiology of TMC OA (Hunter and Wilson, 2009, Koff et al., 2003, Xu et al., 1998). A recent large scale study has found knee morphology, specifically tibial plate slope, was a predictor of OA presentation and progression (Neogi et al., 2013). In order to incorporate representative TMC morphologies into biomechanical simulations to investigate the link between morphology and OA, we must first understand the natural variations in TMC joint shape.

TMC joint OA is common and two to six times more prevalent in women than in men (Acheson et al., 1970, Dias et al., 2007, Haara et al., 2004, Segal et al., 1998, Valdes and von der Heyde, 2012). The sexual dimorphism of the TMC joint bones is believed to play an important role in this discrepancy (Ateshian et al., 1992, Kovler et al., 2004, North and Rutledge, 1983, Xu et al., 1998). Prior studies investigating sex differences in morphology of the TMC joint bones have been focused on the articular surface morphology and range in complexity from simple descriptive classification (Van Nortwick et al., 2013), to measurement of curvature, through the use of dial indicators (North and Rutledge, 1983) and 3D models obtained through stereophotogrammetry (Ateshian et al., 1992, Xu et al., 1998), segmentation of CT images (Conconi et al., 2014, Halilaj et al., 2014b)and laser scanning (Kovler et al., 2004, Marzke et al., 2012). In contrast to previous findings, recent CT-imaging-based studies have found no sex differences in the articular shape of the TMC joint (Conconi et al., 2014, Halilaj et al., 2014b, Marzke et al., 2012). However, there are scarce data concerning the morphology of the entire TMC bones and their variation, in terms of how the bones change or scale across the population. This information has important implications for the scaling of musculoskeletal models, methods for which do not currently account for potential sex differences in morphology (Cooney and Chao, 1977, de Monsabert et al., 2014, Giurintano et al., 1995, Valero-Cuevas et al., 2003, Wohlman and Murray, 2013). Can we assume that a female bone is simply a scaled version of a male bone?

Age is also a factor that might alter the morphology and function of the TMC joint bones. The kinematics of the TMC joint seem to be influenced by age (Halilaj et al., 2014d), which might be due to changes in the morphology of the articular surface (Halilaj et al., 2014b). However, it is not clear whether the entire morphology changes with age in TMC joint bones.

Statistical shape modelling is necessary to quantify the variation in shape across a population (Chan et al., 2013, Fitzpatrick et al., 2011, Van Haver et al., 2014, Zhang et al., 2014) and classify morphological variation by decomposing shapes into a set of statistically significant modes (commonly principal components) (Cootes et al., 1992, Dryden and Mardia, 1998). This is effective for understanding morphology (Bischoff et al., 2014, Vos et al., 2004) and for determining relationships between morphology and parameters of interest, such as sex and age (Anderson et al., 2010, Bischoff et al., 2014, Fitzpatrick et al., 2011). Furthermore, SSMs allow us to investigate specific anatomical regions and examine local shape changes, which can be correlated to parameters of interest or anatomical features, such as ligament or tendon attachment sites.

The purpose of this chapter was to develop a SSM of the trapezial and first metacarpal bones to characterise the size and shape of the whole bones across a cohort of 50. We used this shape model to investigate the effects of sex and age on the size and shape of the TMC joint bones and the articulating surface area of the TMC joint. We hypothesised that women have similar shape trapezial and first metacarpal bones compared to men, following scaling for overall size. We also hypothesised that age would be a significant predictor variable for TMC joint bone changes.

3.3 Methods

CT image data and segmented point clouds of 50 TMC bones from healthy adult males and females were obtained from an on-going study (Halilaj et al., 2014a, Halilaj et al., 2014d). An iterative fitting process involving principal component analysis (PCA) was performed to generate two SSMs: one including size variations and one normalised for size. Statistical analysis of the principal component weights of both SSMs was performed to investigate morphological sex and age differences.

3.3.1 Subject information

After Institutional Review Board approval and informed consent, the dominant wrists and thumbs consisting of 40 right hands and 10 left hands of 50 healthy non-osteoarthritic (radiographic and asymptomatic) volunteers (23 men, age 35.6 year ± 13.7 year and 27 women, age 42.9 year ± 15.3 year) were imaged in a clinical neutral position (Figure 3.1A) with a 16-slice clinical CT scanner (GE LightSpeed 16, General Electric, Milwaukee, WI) to obtain their bone shapes.
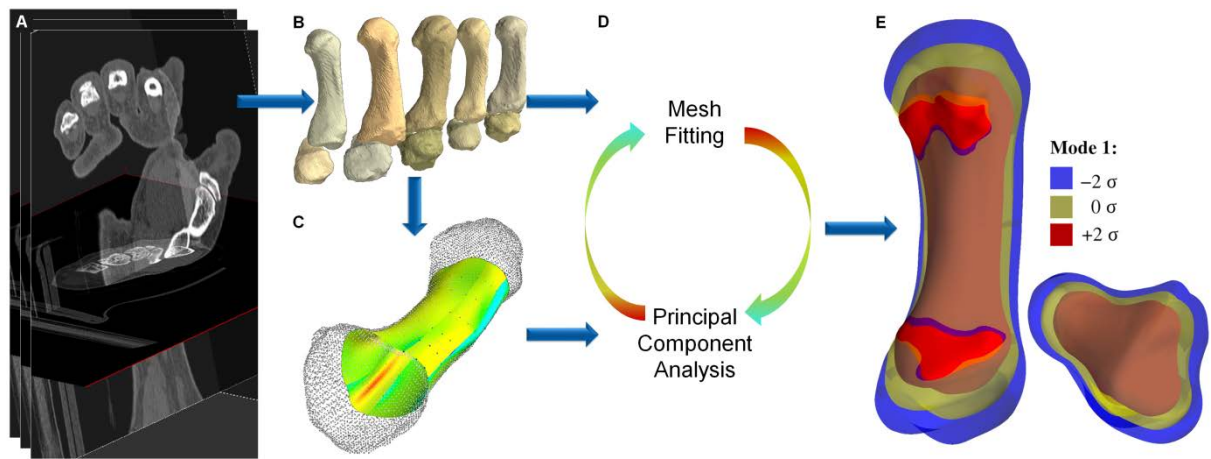
Figure 3.1. Overview of the process for SSM generation. A training set of CT images (A) were manually segmented to produce a triangulated mesh (B). Vertices of a representative triangulated mesh were extracted as a point clouds on which a parametric template mesh (C) was created. The template mesh was fitted to all point clouds in an iterative fitting process (D). The principal components of variation were determined (E).

3.3.2 Imaging protocol

The settings used on the scanner were: tube parameters at 80 kVp and 80 mA, slice thickness of 0.625 mm, and in-plane resolution of 0.4 mm × 0.4 mm. The trapezia and the first metacarpals were segmented semi-automatically by the Department of Orthopedics at Brown University using Mimics v12.11 (Materialise, Leuven, Belgium) and 3D bone models were exported as meshed surfaces (Figure 3.1B). The vertices of these surfaces were extracted to produce a training set of point clouds.

3.3.3 Statistical shape model generation

The technique implemented to generate the SSM for this chapter was based on the work by Zhang et al. (2014). In summary, a custom template cubic-Lagrange piece-wise parametric mesh (Nielsen, 1987) (Figure 3.1C) was created and fitted to all data clouds in the training set via an iterative fitting process (Figure 3.1D). The process involved a series of coarse to fine fits in which the template mesh was initially brought to within 4 mm RMS of the data clouds such that the meshes were close for fitting. Fitted meshes were then rigidly aligned to each other by minimising the least squared distances of corresponding points and PCA (as in section 3.3.5) was carried out on mesh node coordinates to obtain a shape model. This process was repeated 5 times in which the shape model was used to first fit the mesh, thereby propagating fitting correspondence across the training set and finally achieving a RMS error of 0.4 mm. Thus, the shapes of each metacarpal and trapezium of the TMC joint training set were represented by maximally correspondent meshes (Zhang et al., 2014). A final PCA was performed on the nodal coordinates of the training set meshes to yield the SSM (Figure 3.1E) and determine the principal components of variation used in subsequent analysis.

3.3.4 Size normalisation

For SSMs involved in biological systems, size typically dominates the first principal component (Chan et al., 2013, Cootes et al., 1992, Fitzpatrick et al., 2011, Zhang et al., 2014). To investigate pure-shape differences in the trapezia and 1st metacarpal bones between men and women, a general Procrustes analysis (least-squares minimisation of correspondent point differences) was performed on the fitted meshes to filter out scaling variations (Bischoff et al., 2014, Ross, 2004, Stegmann and Gomez, 2002) producing the size-normalised shape model.

3.3.5 Principal component analysis

Principal component analysis was used for dimensionality reduction and allowed any shape, x, in the training set to be approximated as a sum of the mean shape, $\bar{x}$, and the weighted sum of n principal components, ϕ (Heimann and Meinzer, 2009, Zhang et al., 2014):

$$x = \bar{x} + \sum_{i=0}^{n} \omega_i \phi_i \qquad (3.1)$$

where n was chosen such that the accumulated variance explained by the components account for 90 % of the total variation in the population. Thus, the shape of each bone in the training set was described by 8 weights, ω. These weights and the sex and age of the corresponding subjects were used for the following statistical analyses.

3.3.6 Statistical analysis

Principal component weights, which dictate the degree of variation along a principal component, were extracted for the bones of each subject from each shape model and used for t-test against sex, and linear regression was performed against age. For our purposes, it was important to characterise all morphological differences present in the population of TMC joint bones, including both size and shape variations.

3.3.6.1 Characterising size differences

We expected the first principal component of our non size-normalised shape model to be dominated by size variation. Therefore, we extracted the weights of

the first principal component (ϕ_1) for men and women. Q-Q plots and a Shapiro-Wilk test were used to determine normality and a Levene test was carried out to confirm equal variance to satisfy *t*-test assumptions. Finally, *t*-test was performed on the weights classified by sex in conjunction with a boxplot to test if women have significantly smaller trapezia and metacarpal bones compared to men. Linear regression was performed on the weights against age to test for relationships between morphology and age.

3.3.6.2 Characterising Shape Differences

PCA weights from the first five principal components of the size-normalised shape model were used to explore sex and age related pure-shape differences after uniform scale adjustment. After confirming normality and equal variance, *t*-tests with Bonferroni correction were performed on the weights of each principal component, classified by sex to explore if women exhibited significant shape differences to men along each principal component. Linear regression was used to test for relationships between age and morphology.

3.3.7 Articulating surface areas

The articulating surface landmark was identified during parametric template mesh design (Figure 3.1C) where mesh elements were created to segregate the articulating surface and fitted to maximise correspondence.

We expected the articulating surface area to be dependent on both the size and shape. Both shape models were varied by the first principal component weights of the training set and the articulating surface landmark elements were extracted.

Articular surface area means and standard deviations were calculated for men and women. A *t*-test was also performed on the on the surface areas to confirm if the articulating surface areas between the two populations were different.

3.4 Results

3.4.1 Shape model

The first seven principal components of the non size-normalised shape model accounted for over 90 % of the variance in morphology present in the training set (Figure 3.2A). The leave-one-out RMS error for the non size-normalised shape model was 0.4 mm. The RMS error was smaller than the voxel dimensions, indicating a representative shape model with a sufficiently large training set. As expected, the first principal component was size and accounted for 71 % of the variation. The size of the trapezium was linearly correlated ($p < 0.001$) to the size of the metacarpal.
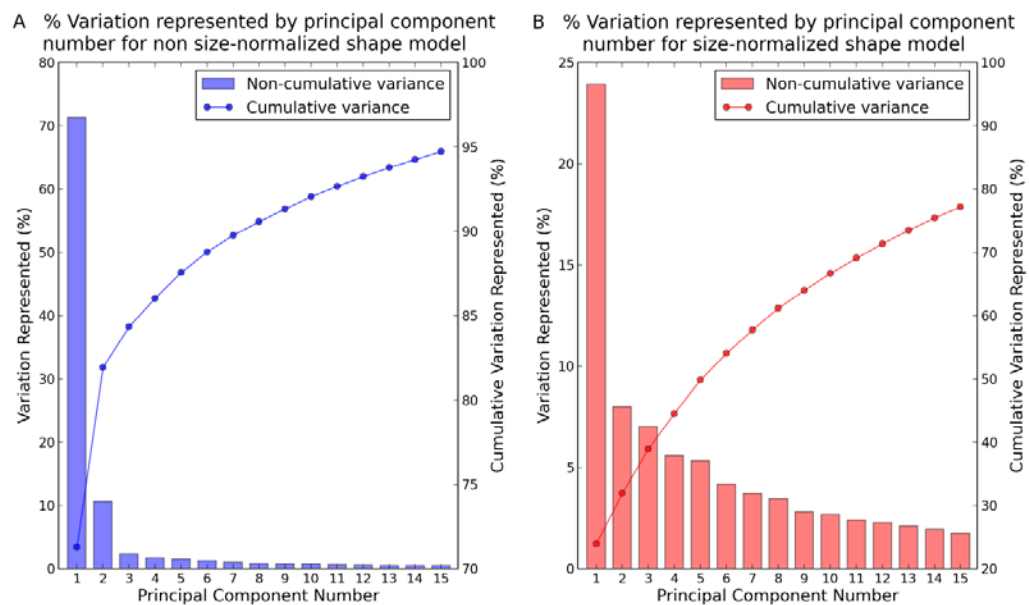
Figure 3.2. Variation and cumulative variation represented by PC number for non size-normalised shape model (A) and size-normalised shape model (B).

3.4.2 Characterising size differences

The trapezial and first metacarpal bones were smaller ($p < 0.001$) in women than in men (Figure 3.3). Correlation of the mode weights with age was poor.

The articulating surface areas of both the trapezial and first metacarpal bones were smaller in women ($p < 0.0001$) than in men (Table 3.1).

Table 3.1. Articulating surface areas in the non-size normalised TMC joint.

Metacarpal	n	Mean area (mm^2)	Trapezium	n	Mean area (mm^2)
Men	23	139.83 ± 13.92	Men	23	149.26 ± 14.54
Women	27	117.67 ± 13.05	Women	27	126.25 ± 13.50
Men vs. Women		*p < 0.0001*	Men vs. Women		*p < 0.0001*
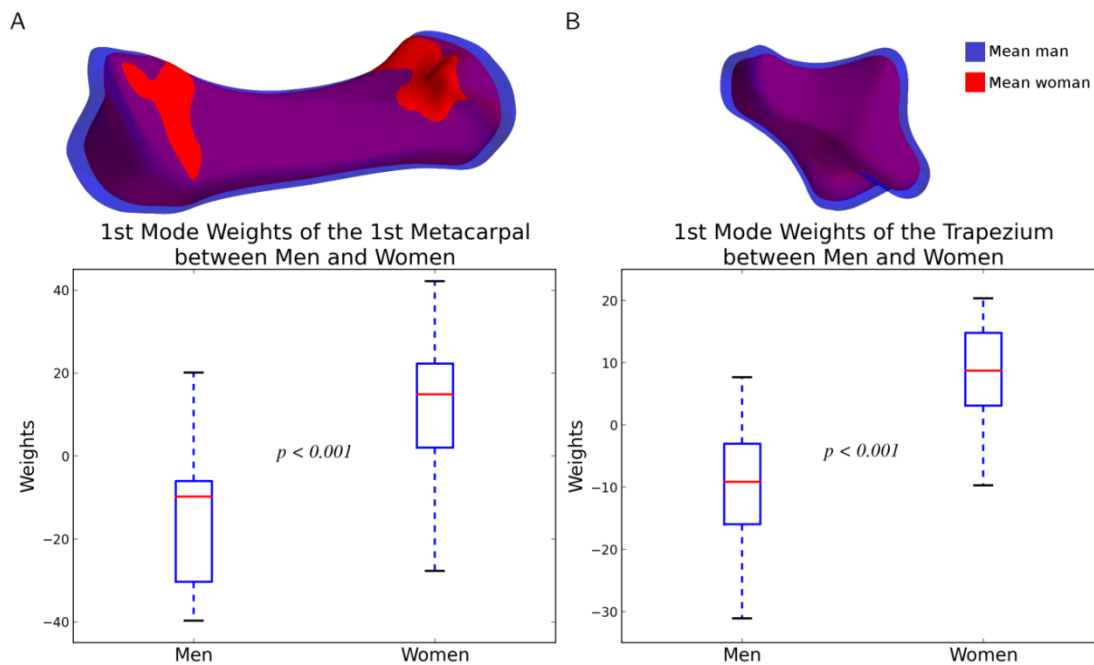
Figure 3.3. Boxplots of mean metacarpal (A) and trapezial (B) bones showing a significant difference (one-way ANOVA p < 0.001) between men and women for first principal component.

The mean first metacarpal bone volume in men was 6101 mm^3 and in women was 4570 mm^3, and the mean trapezium in men and women were 2459 mm^3 and 1755 mm^3, respectively.

Table 3.2.   Mean bone volume in non size-normalised TMC joint.

Mean Bone Volume (mm^3)	n	Metacarpal	Trapezium	Total
Men	23	6101.0 ± 924.2	2458.8 ± 424.3	8559.8 ± 1286.4
Women	27	4569.7 ± 764.3	1755.3 ± 296.5	6325.0 ± 1010.6
Mean Difference		1531.3	703.5	2234.8

3.4.3 Size-normalised shape model

The first seven principal components of the size-normalised shape model for the training set population accounted for approximately 60 % of the variation (Figure 3.2B). The first principal component alone accounted for 24 % of the size-normalised variance present in the training set. For the first metacarpal, this was qualitatively observed as aspect ratio when varied from one extreme to the other (Figure 3.4), where the proximal and distal ends of the first metacarpal moved further apart as the principal component (PC) weights became more positive, and the diameter of the epiphysis became narrower. In the trapezium, the first principal component did not represent aspect ratio. Instead, as the weights became more positive, the radial ridge diminished and the ulnar ridge became more prominent. Changes observed in this mode were very small.
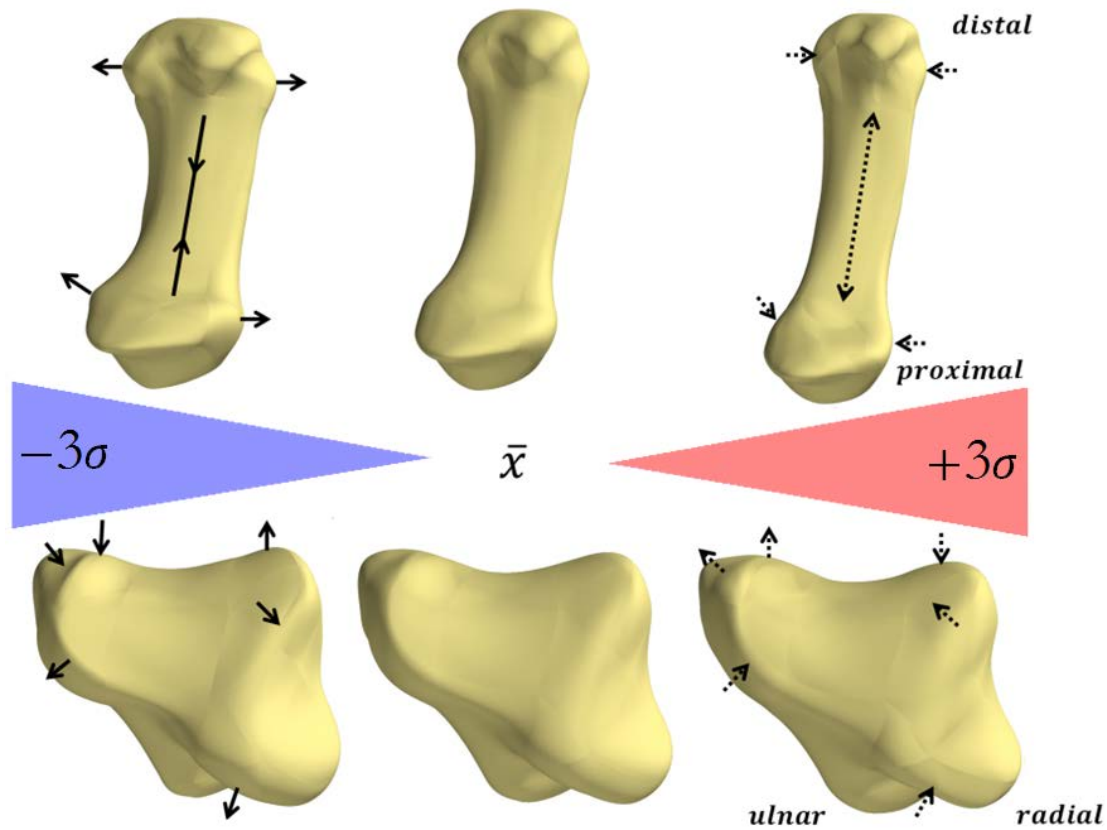
Figure 3.4. Overview of the shape variation exhibited in first principal component of the size-normalised metacarpal and trapezial bones showing the mean ($\bar{x}$) varied by 3 standard deviations (3σ) in the negative direction (men) and positive direction (women).

3.4.4 Characterising pure-shape differences

Since there was a noticeable decrease in the gradient of the cumulative variation curve around the fifth principal component (Figure 3.2B), subsequent principal components were not uniquely and consistently defined. Therefore, investigation of shape differences for these principal components was not performed.

We found a statistically significant difference ($p = 0.01$ after Bonferroni correction) in the weights of the first principal component of the size-normalised shape model between men and women. In women, the first metacarpals had higher aspect ratios, meaning a longer and narrower bone, and the trapezia had a more prominent ulnar ridge (Figure 3.4). None of the first five principal components correlated to age indicating no relationship between

these variables. Though statistically significant, the differences between the men and women as a result of varying the first principal component of the size-normalised shape model were small (less than 1 voxel in magnitude). The difference exhibited a small absolute effect size. Consultation with an orthopaedic hand surgeon revealed that the differences were not clinically significant. These effects were small and could only be distinguished at the extremes of the population (2 to 3 standard deviations away from the mean) (Figure 3.4). E.g. we noted a 2 % difference in trapezial bone volume at 2 standard deviations from the mean.

The articulating surface area of the first metacarpal after size-normalisation remained smaller in women ($p < 0.005$) than in men (Table 3.3). The articulating surface area of the trapezium was larger in women ($p < 0.008$).

Table 3.3. Articular surface areas in the size-normalised TMC joint.

Metacarpal	n	Mean area (mm²)	Trapezium	n	Mean area (mm²)
Men	23	128.36 ± 3.02	Men	23	133.69 ± 0.96
Women	27	126.09 ± 1.75	Women	27	134.34 ± 0.59
Men vs. Women		*p < 0.005*	Men vs. Women		*p < 0.008*

3.5 Discussion

The purpose of this study was to characterise the size and shape of the entire trapezial and first metacarpal bones in a cohort of 50 healthy TMC joints using a SSM. We achieved this by characterising morphological differences in the population of TMC joint bones, including both size and uniform scale adjusted shape variations using two shape models (non size-normalised shape model and

size normalised shape model), and analysing the PC weights in the population. We compared the PC weights between men and women, and performed regression of the PC weights against age. Of the two parameters studied, sex was the only parameter that accounted for differences in PC weights of morphological modes of variation. We found that the only difference in the morphology of the trapezia and first metacarpal bones between men and women was size, thus, confirming our first hypothesis that women and men have similarly shaped trapezial and first metacarpal bones compared to men. Furthermore, we found no correlation between morphology with age and rejected our second hypothesis.

Previous SSMs investigating morphological variation in bones have shown that size dominates the first principal component (Chan et al., 2013, Cootes et al., 1992, Fitzpatrick et al., 2011, Zhang et al., 2014). This was the case in our SSM, where the first principal component accounted for 71 % of the morphological variation in TMC joint bones, which was attributed to size (Figure 3.2). The large reduction in variation from 71 % variation represented in the first principal component to the second principal component, which exhibited 10 % of the morphological variation, suggested that the morphology of the TMC joint bones do not vary much in shape, but instead, mostly vary in size. Bone volumes observed in this study (Table 3.2) were similar to those reported previously (Crisco et al., 2005, Halilaj et al., 2014b, Moore et al., 2007). By varying the size and shape along the first principal component of the non size-normalised shape model, we observed that the size of the TMC joint bones dictated the size of the articulating surface area in both the first metacarpal and the trapezium ($p<0.0001$). As expected, this means that a smaller bone exhibits a smaller articulating surface (Table 3.1). Despite the inclusion of only the first principal component of the non size-normalised shape model, we yielded articular surface areas similar to those reported by Ateshian et al. (1992). This

was not surprising, since most of the variation in the TMC joint bones (71 %) was accounted for by size.

These findings improve upon our current understanding of the TMC joint bones, and have various implications. Firstly, size accounts for the majority of the variation in the TMC joint bones with women having smaller bones on average than men by $\sim$2200 mm^3 (Table 3.2). Size is important when considering the forces, stresses and form-function relationship of the wrist and hand, since scaling of bones influences the action of the ligaments (Nanno et al., 2006), muscles, and the size of the moment arms at joints (Arnold and Delp, 2001). For example, if we consider that the moment arms of muscles crossing the joint would scale with bone size, the forces required to generate the same torques for a given task would be higher in a joint with smaller bones. It has been hypothesised that smaller joints would therefore experience higher stresses due to the smaller articulating surfaces (Kovler et al., 2004, Xu et al., 1998). From our findings, we expect that TMC joints of women with smaller bones would experience higher stresses than men since we expect the forces to be higher and the articular surface areas to be smaller by approximately 15 % (Table 3.1). The effect of size might play an important role in the mechanical aetiology of TMC joint pathology, such as OA. Recent studies have shown that the articular surface is no different between men and women after scaling for size (Conconi et al., 2014, Halilaj et al., 2014b, Marzke et al., 2012). To the author's knowledge, this is the first report suggesting that the shape of the entire TMC joint bones between men and women are similar. The lack of sex difference in shape in the TMC joint suggests that the function of the TMC joint might also be similar between men and women, although further biomechanical analyses would be required to investigate this. A study of a larger cohort with higher imaging resolution would be beneficial to confirm these findings. The implications that men and women have similar shaped TMC joint bones that are simply scaled by size extends from implant design to the scaling

of musculoskeletal models. It would seem appropriate to isotropically scale an implant or model of the TMC joint bones based on overall size, regardless of sex.

We hypothesised that age would be a significant predictor variable for TMC joint bone shape changes. However, since we were unable to find any correlation between age and any of the principal components through linear regression, we must reject our hypothesis based on our methods. A scatter plot of the PC weights indicated that the distribution was random, rather than dependent on age through a linear or non-linear relationship. Our findings suggest that age is a poor predictor of TMC joint morphology, which contrasts with the current literature, where the articular surfaces of the first metacarpal and trapezial bones have been shown to become flatter (lower curvature) and more conforming with age (Halilaj et al., 2014b, Xu et al., 1998). The discrepancies in the results may be due to poor sensitivity of our PCA based SSM to subtle local shape differences. Since we investigated the entire morphology of the TMC joint bones, the ability of the model to capture small variations in articular shape may be compromised. However, the changes observed by Halilaj et al. (2014b) were localised and specific to sub-regions of the articular surface, and is possible to not have been captured in the primary principal components of our SSM.

Although we found a statistically significant shape difference between men and women in our size normalised shape model ($p = 0.01$), we believe this difference to be clinically insignificant in terms of biomechanics and pathology, since average point to point differences in the morphology of the TMC joint bones were small (within 1 voxel) and were only apparent at the extremes of the principal component (2–3 standard deviations from the mean) (Figure 3.4), indicating a small effect size. Also, at 2 standard deviations from the mean, we noted only a 2 % difference in bone volume of the trapezium. Our SSMs represented the segmented data points well to ~0.4 mm RMS (Heimann and

Meinzer, 2009). However, our models do not account for any errors arising from poor imaging resolution or segmentation resolution, which can be a significant source of error. Our higher order meshes should reduce these kinds of resolution-related error by smoothing across data points. Though smoothing may have removed potentially meaningful local detail, when considering the scale of detail which is meaningful, the purpose of our models, and our low RMS error, we believe our model remains valid for its purpose. The overlap of the standard deviation (Table 3.3) and the small effect size lead us to conclude that this finding though statistically significant is not clinically significant, and therefore further reinforces our previous finding that the morphology of the TMC joint bones does not vary in shape, but in size.

Our investigation of the entire morphology of the healthy TMC joint bones is not without its limitations. A high resolution data set would have provided more data points to allow for a more refined mesh such that the SSM could capture more subtle differences in morphology. We assumed that the template mesh landmarks fit well to the anatomical landmarks. This was reasonable since we maximised mesh correspondence through iterative mesh fitting and no artefacts (such as changes in nodal position without changes in mesh geometry e.g. nodal "sliding") were detected in the shape models. Our data consisted of only dominant hands from both left and right handed subjects. The left handed data sets were mirrored to generate consistent training set data. This was deemed as appropriate since we found no difference in morphology between the two groups. Therefore, our study is limited to the characterisation of morphology TMC joint bones in dominant hands and does not characterise those in non-dominant hands. Furthermore, the statistical methods used (such as PCA and linear regression) were not able to discern local and non-linear variation. A local shape model or ICA may be used in the future to analyse local shape variations, while non-linear alternatives to PCA such as Linear Local

Embedding could be used to analyse non-linear variation once a larger dataset becomes available.

We have characterised the morphology of the entire TMC joint bones across a cohort of 50 subjects and investigated the effects of sex and age on the morphology. Our findings confirm our first hypothesis, and suggest that the women have similarly shaped trapezial and first metacarpal bones compared to men, following scaling for overall size. Furthermore, our results reject our second hypothesis, indicating that age is a poor predictor of TMC joint morphology. The findings have important implications for the design of implants for the TMC joint, as well as scaling of musculoskeletal models to investigate function of the TMC joint.

Chapter 4.

Trapeziometacarpal joint contact varies between men and women during three isometric functional tasks

4.1 Abstract

TMC joint OA is widespread and affects women two to six times more than men. The onset and progression of TMC joint OA is believed to be influenced by stresses and strains in the cartilage. The purpose of this study was to characterise sex and age differences in contact area and peak stress location of the healthy TMC joint during three isometric tasks including pinch, grasp and jar twist. CT images from 50 TMC bones from healthy adult men and women were used to create a SSM to parameterise bone meshes in the same frame of reference. FE models with correspondent nodes and elements were created for

each subject and task, and force-driven simulations were performed to evaluate cartilage contact area and peak stress location. We tested for sex and age differences using PCA, linear regression, and LDA. No sex or age differences in contact area were found. We observed sex differences in peak stress location during pinch ($p = 0.0206$), grasp ($p = 0.0264$), and jar twist ($p = 0.0484$), but no age differences. The greatest sex differences were observed during jar twist, where 94 % of peak stresses in men were located in the centre compared with 50 % in the central-volar region in women. These findings show that peak stress locations are more variable in women during grasp and jar twist than men. Women may use different strategies to perform activities of daily living, compared to men, resulting in less consistently located peak stresses.

4.2 Introduction

The TMC joint is susceptible to OA, and women are two to six times more likely to develop TMC OA compared to men (Dias et al., 2007, Haara et al., 2004, Valdes and von der Heyde, 2012). Mechanical factors such as contact forces and contact area are likely to be important contributors to the onset, progression, and sex-disparity of TMC OA (Hunter and Wilson, 2009, Koff et al., 2003, Xu et al., 1998). Prior studies hypothesised that the smaller wrists of women would experience higher stress than men during activities of daily living, such as pinch, grasp, and jar twist, due to smaller contact areas (Ateshian et al., 1992, Schneider et al., 2015, Van Nortwick et al., 2013, Xu et al., 1998). Cartilage stresses and strains are dependent upon both the size and location of the contact area, and these in turn are influenced by the articulating surface geometry, joint posture, and contact forces.

The few studies that have investigated the location of TMC joint contact report contradictory findings. Several studies report contact on the volar-radial side of the trapezium (Halilaj et al., 2015b, Kuczynski, 1974, Napier, 1955, Pieron,

1973), while Eaton and Littler (1969) reported dorsal contact areas, and Ateshian et al. (1995) reported volar-ulnar contact areas. Most of these studies were performed *in vitro* using cadavers and did not consider important factors such as realistic kinematics. Furthermore, the small size and saddle shape of the TMC joint make it unsuitable for Tekscan (Tekscan Inc., Boston, MA, USA) or pressure film experiments, making direct measurement of contact pressure location difficult. Halilaj et al. (2015b) investigated different postures *in vivo*, but used a surrogate measure (joint space centroid) to infer joint contact. To understand the contact area and peak stress location in the TMC joint, and how these locations differ between men and women, the articulating surface geometry and joint kinematics should ideally be accounted for. This can be performed using a suitable computational model with medical imaging data such as clinical CT scans of quasi-static poses.

We recently performed a statistical shape modelling study using CT scans from a cohort of 50 individuals and found that the trapezial and first metacarpal bones of men and women differed only in size and not in shape (Schneider et al., 2015). These results suggest that size alone is a key difference between the TMC joints of men and women. However, the resulting contact area is influenced by the orientation of the bones during a functional task. Halilaj et al. (2014d) reported that the variability in TMC joint kinematics is large, but found no statistical difference between men and women. In their study, older subjects had 2° greater adduction-abduction compared to younger subjects during pinch, grasp, and jar twist tasks. *In vivo* kinematic and morphological integration will benefit our understanding of contact area and peak stress location in the TMC joint as it relates to OA development.

The purpose of this study was to characterise sex and age differences in the contact area and peak stress location of the TMC joint cartilage during pinch, grasp, and jar twist. To achieve this we developed a parameter optimisation

method using population-based FE models to evaluate cartilage contact in a cohort of 50 subjects.

4.3 Methods
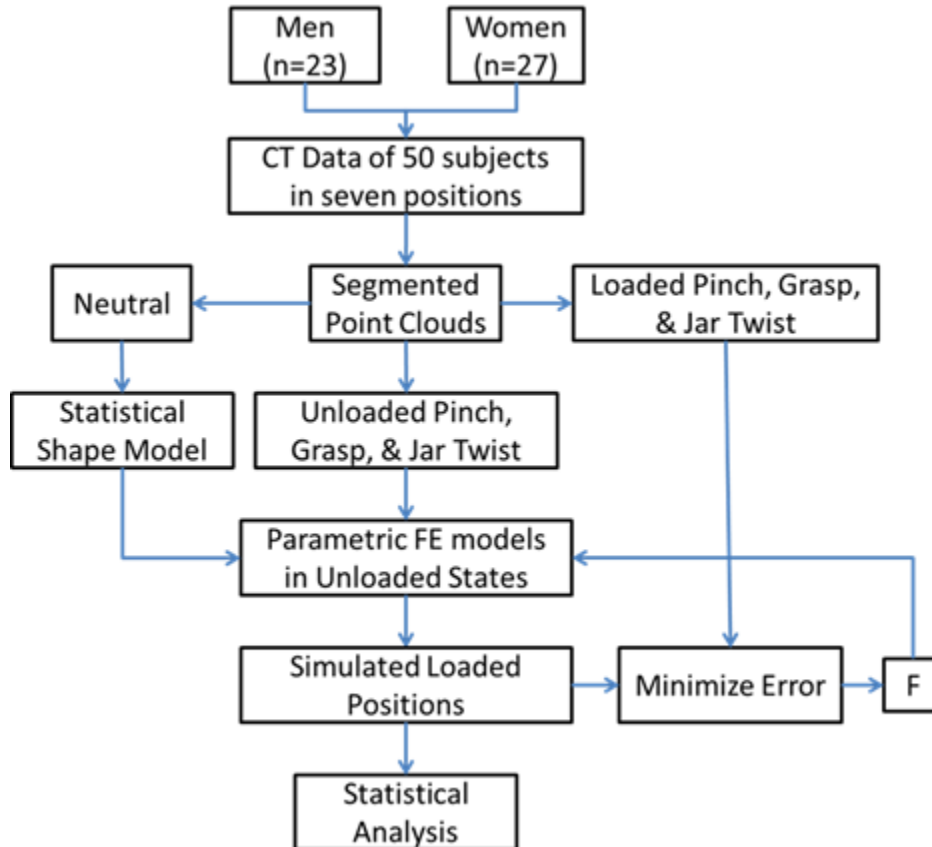
Figure 4.1. Overview of the method: Clinical CT of 50 healthy adult men and women in seven positions (including neutral, unloaded pinch, unloaded grasp, unloaded jar twist, loaded pinch, loaded grasp, and loaded jar twist) were segmented into point clouds. Neutral point clouds were used as a training set to create a SSM of the bones. The SSM was used to create parametric FE models of the trapezial and first metacarpal bones and were initialised in the unloaded state. Force-driven FE simulations were performed to simulate the loaded posture. The force vector, F, was optimised to minimise the error between the simulated postures and the actual loaded posture from CT. The results were analysed statistically.

4.3.1 Subject information

Data from an ongoing study was obtained for this analysis (Crisco et al., 2015a, Halilaj et al., 2014b, Halilaj et al., 2015b, Halilaj et al., 2014d, Schneider et al., 2015). After Institutional Review Board approval and informed consent, the dominant wrists and thumbs consisting of 40 right hands and 10 left hands of 50 healthy non-osteoarthritic (radiographic and asymptomatic) volunteers (23 men, aged 35.6 year ± 13.7 year and 27 women, aged 42.9 year ± 15.3 year) were imaged with a 16-slice clinical CT scanner (GE LightSpeed 16, General Electric, Milwaukee, WI) (Figure 4.1) (Halilaj et al., 2014d). Prior to enrolment, an orthopaedic surgeon examined each subject to rule out conditions that alter TMC joint morphology or kinematics, such as inflammatory arthritis, metabolic bone disease, traumatic injury, surgery, signs of TMC or hand OA, or other non-osteoarthritic diseases of the hand (Crisco et al., 2015a, Halilaj et al., 2014b, Halilaj et al., 2015b, Halilaj et al., 2014d, Schneider et al., 2015).

4.3.2 Imaging protocol

Each subject was imaged in seven positions with custom rigs (Halilaj et al., 2014d). The seven positions included clinical neutral position, unloaded pinch position, loaded pinch position at 80 % maximum effort, unloaded grasp position, loaded grasp position, unloaded jar twist position, and loaded jar twist position (Halilaj et al., 2014d). The settings used on the scanner were: tube parameters at 80 kVp and 80 mA, slice thickness of 0.625 mm, and in-plane resolution of 0.4 mm × 0.4 mm. The mean total radiation burden from seven scans for each subject was approximately 0.35 mSv. The trapezia and the first metacarpals of the neutral position were segmented semi-automatically using Mimics v12.11 (Materialise, Leuven, Belgium) and automatically registered to the TMC bones of the CT images in the other six positions. 3-D bone models

were exported as meshed surfaces and the vertices of these surfaces were extracted to produce a training set of point clouds for SSM generation.

4.3.3 Statistical shape model generation

Methods from a previous study were used to generate our SSM for parameterising the TMC bones (Schneider et al., 2015, Zhang et al., 2014). In summary, a custom template mesh with cubic-Lagrange elements (Nielsen, 1987) was designed to preserve articular surface boundaries of TMC joint bones. This template mesh was fitted to all data clouds in the training set via an iterative fitting process to produce maximally correspondent (parametric) bone meshes. PCA was performed on the correspondent meshes to create the SSM.

4.3.4 FE mesh generation

Metacarpal and trapezial bone FE meshes were generated by discretising the higher order cubic Lagrange meshes obtained from the SSM into triangulated simplex meshes that were compatible with the FEBio (Maas et al., 2012) solver.

The articular surface region of the bone mesh was discretised to create a quadrilateral mesh, which was embedded in the SSM such that the mesh would morph with the shape model. Since the TMC cartilage was not visible in the CT images, the cartilage meshes for each subject were obtained by extracting the quadrilateral mesh from the SSM of each TMC bone, and lofting a uniform thickness (Koff et al., 2003) (0.7 mm) normal to the surface to create a hexahedral cartilage mesh three elements deep. A convergence test with 4 elements found little difference in the contact area (RMS Error < 1.7 mm^2) and location of peak stresses (RMS Error < 0.5 mm), which indicated that 3 elements were sufficient for our purposes (Anderson et al., 2008).

4.3.5 Finite element model

A custom python script was used to prepare the FE model to be solved by FEBio (Maas et al., 2012) for each dataset performing each task. For each task the posture of the TMC joint bones was initialised in the unloaded position with the centroid of the trapezium fixed at the origin (Figure 4.2). The joint was aligned such that the vector from the centroid to a landmark on the radial side of the trapezium was aligned with the x-axis (flexion-extension axis), and the vector from the centroid of the trapezium to the centroid of the metacarpal was aligned with the z-axis (internal-external rotation axis), and the cross-product of these two vectors was aligned with the y-axis (abduction-adduction axis).

The kinematics of cartilage deformation was based on finite, or large, deformation theory. Since we were not interested in time-dependent dynamic effects, cartilage was treated as an elastic material. The stress-strain relationship of the cartilage was described using the neo-Hookean constitutive law. The stress-strain derived from this constitutive model exhibits a linear relationship at small strains but deviates from the linearity and becomes non-linear for relatively larger strains. The parameters used in the constitutive model were: Young's modulus = 10 MPa and Poisson's ratio = 0.4 (Blankevoort et al., 1991, Büchler et al., 2002, Kempson, 1980). The deformed state of tissues for each task was obtained by solving the weak form of the governing equation derived from the principle of virtual work over the discretised (FE) domain with boundary conditions (net muscle force) and contact constraints (between cartilage layers) in place. Contact was imposed using an augmented Lagrangian method (Maas et al., 2012). Subsequently, the displacement, contact area and strain energy density (SED) of each tissue layer were calculated.

Cartilage meshes were tied using the augmented Lagrangian method to the subchondral surfaces of the corresponding bones which were modelled as rigid bodies (Maas et al., 2012). The trapezium was fixed in all degrees of freedom,

while the metacarpal was unconstrained in all 6 degrees of freedom. A force vector representing the summed muscle and joint contact forces was passed through the centroid of the first metacarpal towards the trapezium to bring the two cartilage surfaces into contact. We assumed no contribution from ligaments during these postures.
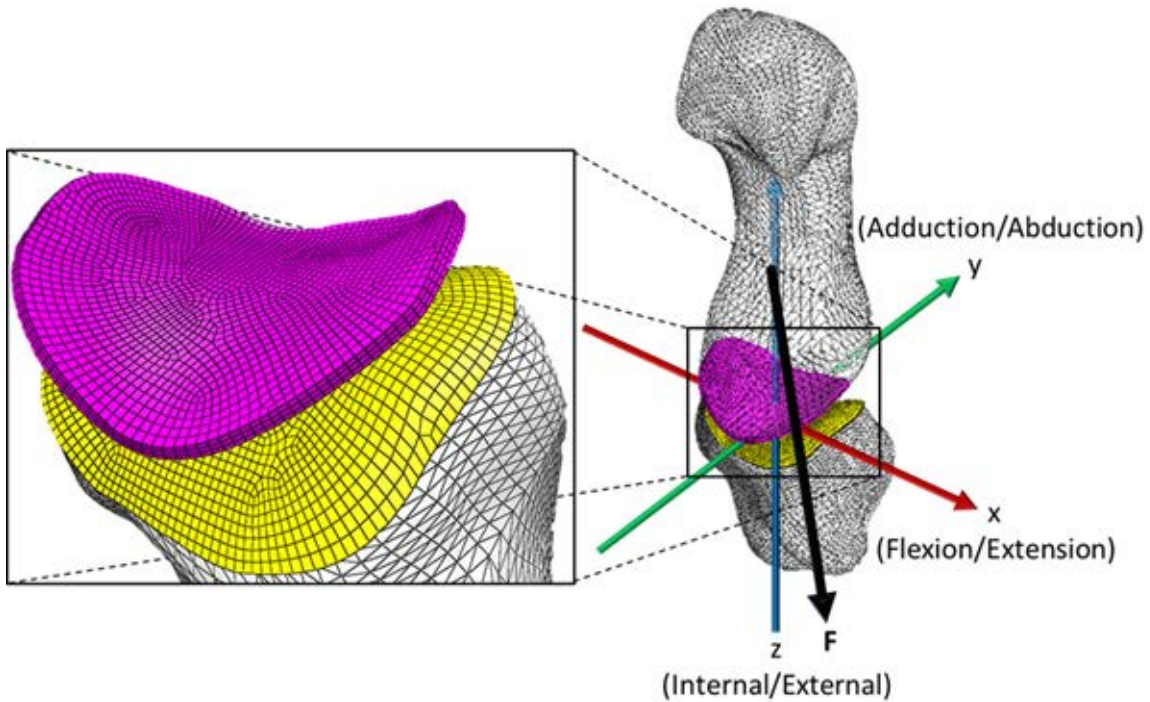
Figure 4.2. FE model showing: an unconstrained first metacarpal, fixed trapezium, coordinate system (x,y,z) aligned with the kinematic axes, and the force vector (F) passing through the centroid of the metacarpal towards the trapezium.

4.3.6 Parameter optimisation

Because we did not explicitly model the muscle forces for each simulation, we performed an optimisation to identify a force vector that allowed the simulated loaded posture of the metacarpal with respect to the trapezium to be in the same position and orientation as that measured in the loaded CT scan. To achieve this, a custom python library was used to export the FE model to a file format compatible with FEBio (*.feb). FEBio v2.4 was used to solve for the

displacements, contact area, and resulting cartilage stress (here we used SED as a stress invariant) during contact as a result of the force vector. We used a bounded BFGS nonlinear minimisation algorithm to optimise for the force vector that minimised the corresponding RMS error between the nodes of the first metacarpal in final simulated position, and the nodes of the first metacarpal in segmented loaded position for each task. Simulations with a RMS error larger than 0.5 mm, or exhibited edge loading, were omitted from the statistical analysis.

4.3.7 Statistical analysis

4.3.7.1 Contact area

We performed a linear regression between contact area (predicted from the FE simulation), and age for each task. We also performed a t-test between contact area and sex for each task.

4.3.7.2 Peak stress location

We extracted the stress distribution of all subjects, normalised the distributions to the peak stress such that we could compare the distributions parametrically (Figure 4.3A), and performed PCA on the normalised stress for each task (Figure 4.3B). We performed a linear regression between the PCA weights and age. Next, we performed a LDA on the PCA weights for each task against sex (Figure 4.3C). LDA classified men and women as positive and negative LDA weights respectively. A t-test was performed between the LDA weights of men against those of women. We explored the minimum number of PCA modes to include in the LDA to classify men and women successfully. This was done to

prevent over-fitting and was achieved by comparing the number of modes included, the LDA score, and the p-values. Finally, we reconstructed spatial frequency plots of contact for each group (Figure 4.3D) by shifting along the normal vector to the hyperplane that separates the PC weights between men and women until we had 100 % classification accuracy for that sex. Contact was defined as elements that exhibited positive SED. These plots show the expected contact for each group, reconstructed with the minimum number of modes that display a significantly different distribution between groups ($p < 0.05$). The minimum number of modes was selected to avoid both over-fitting in the model and the introduction of noise.

4.4 Results

Average simulation convergence RMS errors for pinch, grasp, and jar twist were 0.293 mm, 0.325 mm, and 0.405 mm respectively. These errors were within the spatial resolution of the CT scans. Simulated forces were between 400-1000N depending on subject and task.

4.4.1 Contact area

Results from linear regression indicated that age was a poor predictor of contact area (pinch $R^2 = 0.0197$, grasp $R^2 = 0.0214$, jar $R^2 = 0.0195$). We found no differences in the contact area between men and women during the three isometric tasks (Table 4.1). We found differences in the contact areas between pinch and grasp ($p = 0.0003$), and pinch and jar twist tasks ($p = 0.0002$).
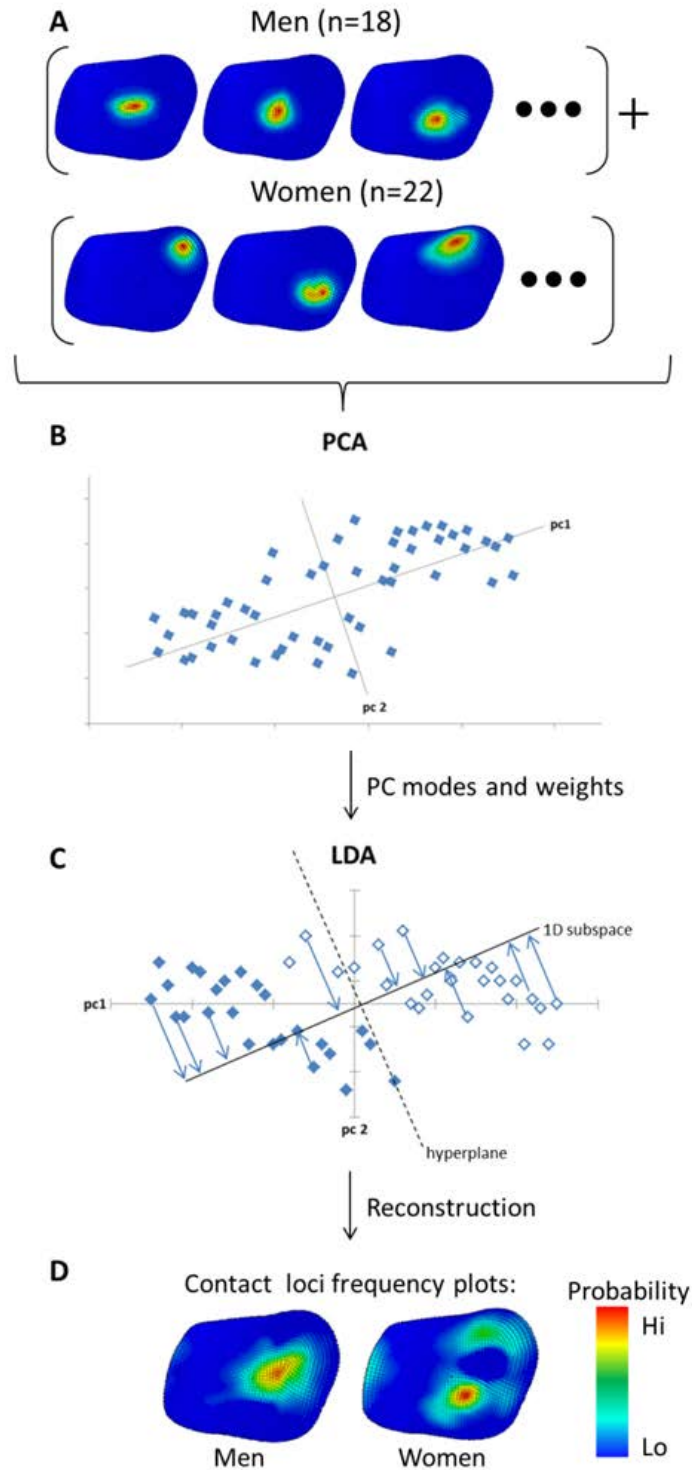
Figure 4.3. Overview of the process used for analysing differences in cartilage stress distributions between men and women for jar twist. Cartilage stress distributions were normalised by peak stress (A). PCA was performed on the set of normalised distributions (B) to produce PC modes and weights. LDA of PC weights classified sex differences (C). LDA weights were used to reconstruct classification criteria for men and women (D). Red indicates a high probability of contact, and blue indicates a low probability.

Table 4.1. Mean (± standard deviation) contact areas in the trapezial cartilage of the TMC joint during pinch, grasp and jar twist for men and women. Note that the number of simulations (n) for each condition was not consistent due to some simulations being omitted (as described in methods).

	Pinch		Grasp		Jar Twist	
	n	Area (mm^2)	n	Area (mm^2)	N	Area (mm^2)
Men	16	20.85 ± 5.91	19	11.90 ± 6.04	18	14.91 ± 4.77
Women	17	19.93 ± 4.90	20	13.00 ± 6.24	22	12.83 ± 4.34
Men vs. Women		$p = 0.639$		$p = 0.590$		$p = 0.167$

4.4.2 Peak stress location

We found no correlation between age and peak stress location for all tasks. We found sex differences in the peak stress location during all three tasks. The inclusion of more modes in the LDA had two effects. Firstly, classification accuracy (LDA score) increased, and secondly, p-values from *t*-tests between the LDA weights of men and women decreased (Figure 4.4). Four, five, and six PC modes were the minimum number of modes required to classify a difference between men and women (*p*-value < 0.05) for pinch (*p*-value = 0.0206), grasp (*p*-value = 0.0264), and jar twist (*p*-value = 0.0484), respectively, without overfitting.
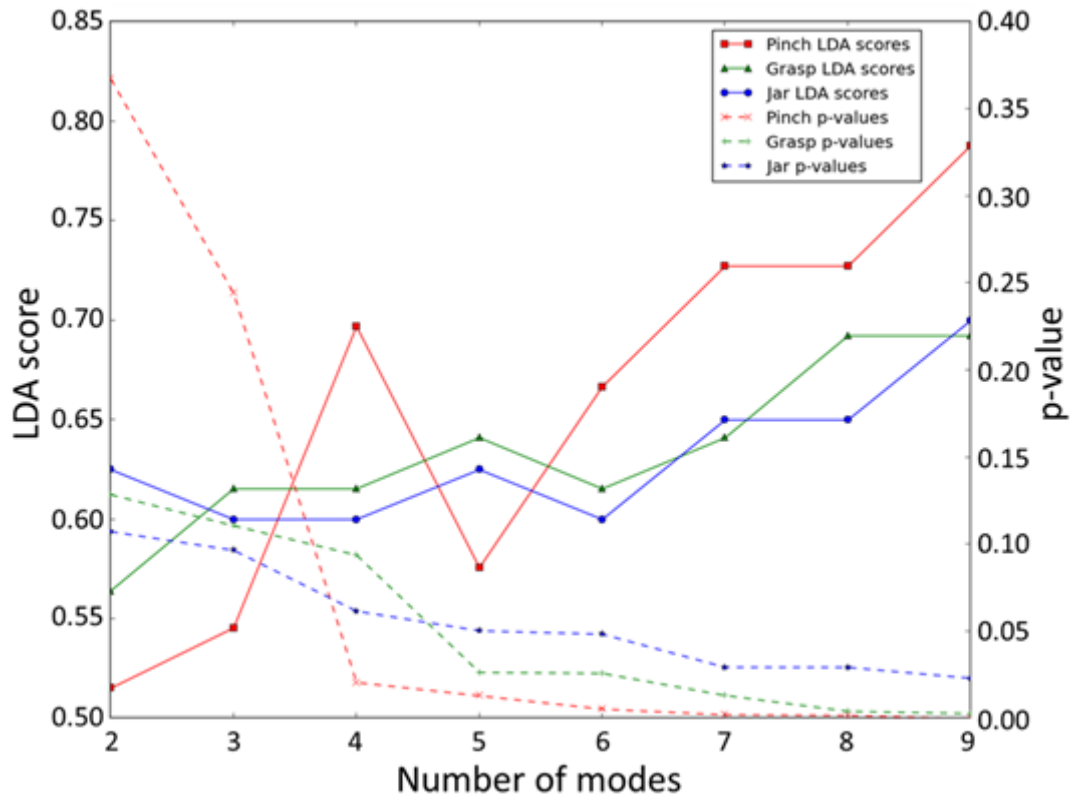
Figure 4.4. LDA score, and p-value between men and women, against number of modes for pinch, grasp, and jar twist. The minimum number of modes that are required for the LDA model to classify a difference ($p < 0.05$) in location of contact between men and women for pinch, grasp, and jar twist, was four, five and six modes, respectively.

For all three isometric tasks considered, the frequency plots of peak stress location between men and women show peak cartilage stress in different regions of the joint (Figure 4.5). For women performing pinch tasks, peak contact stress was located centrally in 53 % of women, with some spread to the radial-volar region and ulnar region. In men, 44 % of pinch contact was located central radially with some dorsal spread. A smaller percentage (19 %) of men experienced contact close to the ulnar ridge.
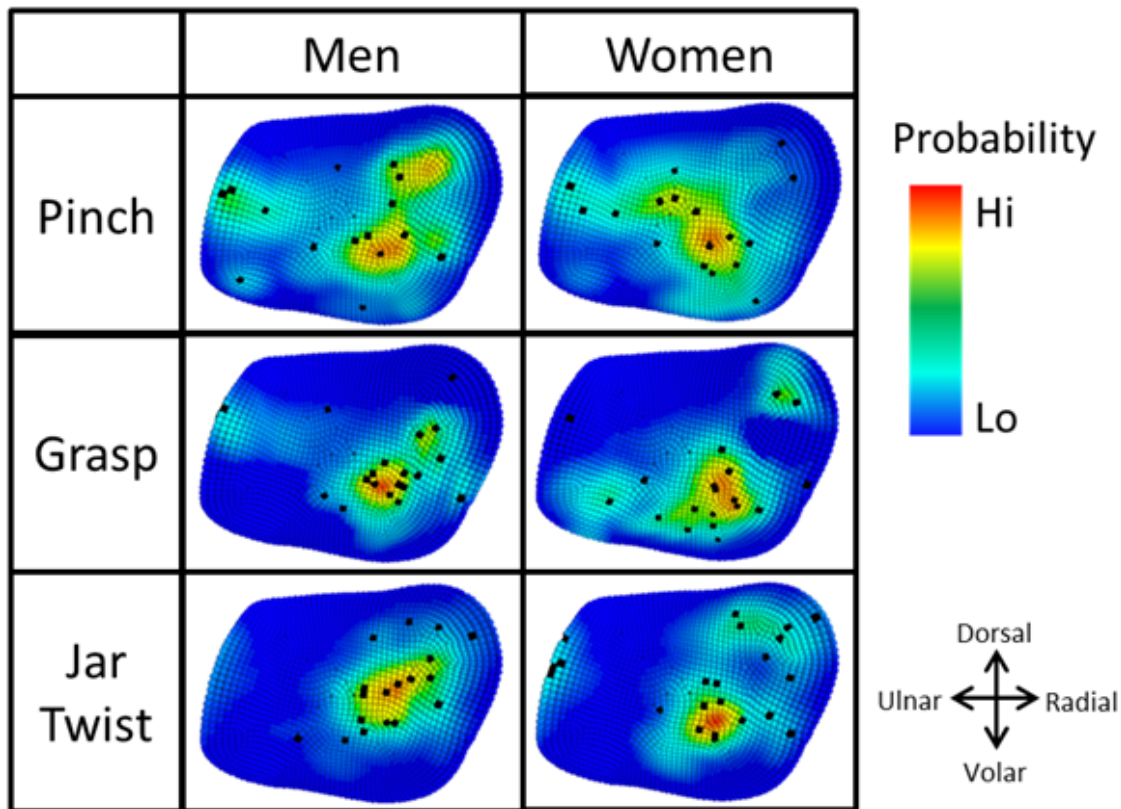
Figure 4.5. Expected locations of peak cartilage stress in men and women for pinch, grasp, and jar twist, where red indicates the most likely location of peak stress and blue indicates the least likely location of peak stress. Black points indicate location of peak cartilage stresses in individual subject FE models.

Peak stress locations during the grasp task were more consistent than during pinch for men, as indicated by the focused frequency plot (Figure 4.5). In men, the majority of contact occurred radial from the centre (68 %), with 5 % experiencing contact at the ulnar region. In contrast, location of peak contact stress during grasp in women was less consistent and found in one of three regions. In decreasing order of frequency, these were the radial-volar region (60 %), the dorsal-radial region (10 %), and the ulnar-volar region (10 %), with 20 % scattered across the remaining region.

Of the three tasks tested, jar twist produced the most consistent results in men, with 94 % of peak cartilage stress located in a central to dorsal-radial spread. In contrast, women experienced three regions of contact. In decreasing order of

frequency, these were the central-volar region (50 %), the dorsal-radial region (32 %), and the ulnar region (18 %).

4.5 Discussion

The purpose of this study was to determine sex and age differences in the contact area and peak stress locations of the TMC joint cartilage during pinch, grasp, and jar twist. Our study used a SSM, FE modelling and parameter optimisation, as well as data reduction techniques on a population of healthy men and women to investigate sex differences in contact in silico. Our findings show that the apparent natural variation in peak stress location is higher in women during grasp and jar twist tasks than in men (Figure 4.5). Our findings show that men and women exhibit differences in the location of peak cartilage stress for all three isometric tasks studied. However, contact area was not significantly different between men and women during these tasks. Furthermore, age was a poor predictor of contact area and peak stress location. Our findings show a difference in the peak stress location between men and women during pinch (Figure 4.5). For pinch, the most common peak stress location in men was in the central-radial region of the cartilage with some spread to the dorsal-radial region. This finding was consistent with the dorsal-radial contact areas reported by Ateshian et al. (1995). However, these investigators also reported volar-ulnar contact areas during pinch, which was only exhibited in 6 % of men. Although 6 % of women experienced contact in the volar region, pinch contact in women was primarily located in the centre, consistent with the work of Halilaj et al. (2015b). Our results disagree with the reports of primarily palmar contact areas during lateral pinch (Pellegrini et al., 1993). The variation in pinch peak stress location might be explained by the higher overall motion (5° in pinch, compared to 0.5° to 2° in grasp and jar

twist) involved in performing pinch and the high variability (s.d. of $\pm 8°$) in pinch kinematics across the population (Halilaj et al., 2014d).

Current TMC literature is limited in descriptions of the contact area and peak stress location for grasp and jar twist tasks. To the authors' knowledge, the study by Halilaj et al. (2015b) is the only report which has estimated contact locations using joint space centroid. Using a FE method, we estimated locations of peak stress within the cartilage, which we believe is an important parameter to understand the potential degeneration of the tissue. Men and women exhibited different locations of peak stress during grasp and jar twist tasks. During grasp, the majority of men experienced contact in the central-radial and central-volar regions. This is consistent with contact locations reported by Halilaj et al. (2015b) In contrast, peak stress locations in women were less consistent during grasp, indicating a greater variability in how this task was performed among women.

Jar twist tasks performed by men produced the most consistent peak stress locations in this study. Halilaj et al. (2015b) found contact to consistently occur in the central-radial region for all men, which is in agreement with our peak stress results. In contrast, peak stress locations in women varied more (Figure 4.5). One possible explanation for the greater variability in peak stress locations is that since women have smaller hands and TMC joint bones (Schneider et al., 2015), and the jar and grasp rigs were of a fixed diameter (Halilaj et al., 2014d), different kinematics were required to execute the same task. This is often the case with activities of daily living where object size is constant and does not scale with hand size. When analysing the kinematics involved in jar twist, Halilaj et al. (2015b) found a difference of six degrees in the abduction-adduction between men and women which might explain why peak stress location was more variable in women than in men (Halilaj et al., 2014d). Muscle weakness, poor neural coordination and pre-pathological kinematics might also be

responsible for this difference. However, considering our healthy subjects, without further investigation we can only conclude that the apparent natural variation in peak stress location for these tasks is highly variable, especially amongst women.

Although men had greater bone size compared to women, contact area was not different between men and women (Schneider et al., 2015). Contact areas in men and women performing the same tasks overlapped significantly, but were different across tasks (Table 4.1). This suggests that size of the contact area does not depend on bone size, but depends on the posture of the joint during contact.

Both men and women experienced peak cartilage stress in regions that correlate to known wear patterns observed in TMC OA. Momose et al. (1999) reported that degenerative change was frequently observed in the radial, volar (Xu et al., 1998), and ulnar regions of the trapezium. The primary location of peak stress in women performing grasp was the volar-radial region (Figure 4.5), which was reported to be the quadrant with most significant cartilage wear in TMC OA (Koff et al., 2003). Location of peak stress on the ulnar side was not common, but occurred in a minority of men during pinch and grasp, and in women during pinch, grasp, and jar twist. During pinch, 19 % of men, and 18 % of women experienced peak stress in the ulnar region, whereas in grasp, 5 % of the peak stress in men and women was located ulnarly, and 18 % of peak stress during jar twist was located in the ulnar region in women. This loading profile correlates with known wear patterns in the ulnar region of the trapezium (Momose et al., 1999). These results suggest that several subtypes of thumb OA may exist, explaining outlier contact zones with varied tasks in both sexes. Cartilage degeneration may occur through divergent mechanisms rather than a single progression pattern (Van Nortwick et al., 2013).

The strengths of our method include identifying the differences in peak stress locations between men and women in silico, and visualising the spatial spread of the expected contact location for each group. Although our findings were consistent with the work of Halilaj et al. (2015b), our unique method allowed our results to provide supplementary and quantitative information regarding the cartilage stress and the distribution of cartilage stress across the joint. Second, since our results were obtained through solving force-controlled mechanics problems (with all degrees of freedom unconstrained), the joint postures, contact areas, and contact locations calculated were not susceptible to small errors in kinematics. In contrast, prescribing displacement boundary conditions for a small joint with thin cartilage often results in non-physiological forces. Lastly, our method of using a parametric mesh derived from a population model allows us to compare FE results from individuals within the population in the same reference frame. This allows us to compare high resolution contact data parametrically, without the need for grouping data into quadrants, and simplifies future surrogate models to represent cartilage stress.

Our method also has several limitations, which are worth mentioning. Firstly, the data collected were from static, isometric postures of the TMC joint during 80 % maximum pinch, grasp, and jar twist and may not represent the typical forces produced during dynamic activities of daily living. Rather than explicitly model the muscle and joint contact force, we optimised a force vector which stabilised the TMC joint in the imaged orientation. The final optimised force vectors were of a reasonable magnitude. The assumption underlying this method was that the final static orientation and position of the metacarpal is a result of the combined muscle and joint contact force with no contribution from ligaments. This assumption is justified as prior studies show TMC ligaments to be lax during the ranges of motion studied (Halilaj et al., 2015c). Since the TMC cartilage was not visible in the CT images, we represented cartilage as a uniform thickness of 0.7 mm with neo-hookean properties. Thus,

variation in the cartilage height distribution has been neglected. We considered this assumption to be reasonable since Koff et al. has previously shown that the cartilage in early osteoarthritic (stage I) and even stage II and III osteoarthritic TMC joints exhibited less than 10 % variation in cartilage thickness across quadrants (Koff et al., 2003). Similarly, Conconi et al. (2014) assumed that the subchondral bone was a reasonable measure for calculating joint congruence distribution in the neutral position using a contact based congruence measure. In healthy TMC cartilage, the mean thickness is less than 1 mm, and variation from the mean is small enough to not significantly affect the outcomes of a force controlled FE analysis. Thus, our findings appear to give reasonable characterisation of peak stress location and contact area size. Furthermore, using a hip joint model, Anderson et al. (2010) showed that predicted cartilage contact pressure magnitudes and distributions were comparable when using a FE model with subject-specific cartilage geometry compared to a FE model with uniform cartilage thickness, so long as the underlying bone geometry was accounted for. At the ankle joint, Anderson et al. (2007) generated a cartilage contact model by uniformly extruding cartilage elements from a bone surface obtained from CT data and showed close agreement with measured pressure distributions from Tekscan data. We tested the effect of varying the cartilage thickness within ± 0.2 mm throughout the study and did not find a clinical difference in the investigation of sex and age differences in contact area size (RMS Error < 2.5 mm^2) and location (RMS Error < 1.2 mm^2). Another limitation was that we modelled the subchondral bones as a rigid body. This was justified as cortical bone properties range between 10-20 GPa, whereas cartilage properties are approximately 10 MPa. We do not believe that the contact area size and location or peak stress location would be significantly affected by modelling the bone as deformable, as cartilage properties are orders of magnitude lower than cortical bone, resulting in an interaction that is similar to one with a rigid body. Lastly, we do not believe that the contact area size and

location would be significantly affected by a more complex constitutive model of cartilage (e.g. Mooney-Rivlin) (Maas et al., 2012).

Our findings show that the location of peak cartilage stress in the TMC joint of men and women performing pinch, grasp, and jar twist tasks are different; men perform the tasks more consistently than women during grasp and jar twist. Contact areas do not appear to vary with age or sex, but are dictated by the task being performed. Furthermore, a subset of peak cartilage stress locations have been correlated with known wear patterns. This work has implications in terms of musculoskeletal modelling, understanding joint pathology, and tools that may potentially aid in clinical diagnosis of joint disorders. We envision a clinical tool which can automatically predict and diagnose joint degeneration based on morphology, kinematics and patient demographics. Further work should evaluate the kinematics of subjects that produce atypical cartilage stress locations and to evaluate and compare to subjects with early OA.

Chapter 5.

Early morphologic changes in trapeziometacarpal joint bones with osteoarthritis

The following is a reproduction of the article (In review):

5.1 Abstract

Characterising the morphological differences between healthy and early osteoarthritic TMC joints is important for understanding OA pathology, and early detection is important for treatment and disease management. This chapter has two aims: first, to characterise morphological differences between healthy and early osteoarthritic (EOA) TMC bones. The second aim was to determine the efficacy of using a SSM to detect early signs of OA. CT image data of 50 TMC bones from asymptomatic volunteers and 75 patients with EOA were obtained from an ongoing study and used to generate a SSM. A

LDA classifier was trained on the PC weights to characterise features of each group. Statistical analyses were performed on the PC weights, and LDA weights to investigate differences in morphology. Leave-one-out classification was performed to evaluate the ability of the LDA classifier to detect the early signs of EOA. We found that TMC bones of EOA subjects exhibited a lower aspect ratio ($p = 0.002$) compared with healthy subjects. The LDA classifier determined that protrusions (mean size = 2.5 mm) at the volar beak of the first metacarpal were characteristic of EOA subjects ($p < 0.001$). This was accompanied with widening of the articular surface, deepening of the articular surface, and protruding bone growths along the concave margin. These characteristics resulted in a classification sensitivity of 82.7 % and specificity of 71.4 %. Our findings indicate that morphological degeneration is well underway in the EOA TMC joint, and shows promise for a clinical tool that can detect these features automatically.

5.2 Introduction

TMC joint OA is widespread and involves degeneration of the bone and cartilage with aging (Armstrong et al., 1994, Haara et al., 2004). Aetiology of TMC joint OA is unclear, but biomechanical factors have been identified as important contributors to the onset and progression of OA (Baker-LePain and Lane, 2010, Beck et al., 2005, Hunter and Wilson, 2009, Kim et al., 2006, Neogi et al., 2013, North and Rutledge, 1983, North and Eaton, 1983).

Morphology is an important biomechanical factor that plays a role in contact mechanics, and has been hypothesised to play a role in the development and progression of TMC OA. Furthermore, kinematics of the TMC joint and cartilage stress and strain are dependent on the morphology of the articulating bones. Neogi et al. (2013) discovered that bone shape could predict the onset of OA in the knee, often several years before onset of OA. Baker-LePain and

Lane (2010) reported that joint shape was an important determinant of OA in the hip, and is in turn affected by OA, leading to a complicated interaction between morphology and disease. In the hip, several morphological factors, such as acetabular dysplasia, acetabular retroversion (Kim et al., 2006), pistol grip deformity, wide femoral neck, altered femoral neck-shaft angle, cam and pincer impingement (Beck et al., 2005), appear to play an important role in the pathogenesis of OA and may precede the development of OA by decades. In the TMC joint, the morphology of the articulating surfaces remains the prevailing explanation for the aetiology of TMC joint OA (Ateshian et al., 1992, Bettinger et al., 2000). Early detection of osteoarthritic changes would allow clinicians to have the best chance of reducing the impact of the disease by providing alternative treatment options.

Existing studies investigating the three dimensional morphology of the trapezial and first metacarpal bones have many limitations. These include small sample sizes (Ateshian et al., 1992, Kuczynski, 1974), qualitative binning (North and Eaton, 1983), use of simplified 2D morphometrics (North and Rutledge, 1983, Smith and Kuczynski, 1978, Van Nortwick et al., 2013), restricted to only the articular surface (Conconi et al., 2014, Halilaj et al., 2014b), and thus do not capture the spectrum and complexity of 3D shape changes involved in the entire TMC joint with the onset of OA. Morphological analysis has not been performed in the same frame of reference, and has been limited to osteoarthritic TMC joints (Koff et al., 2003, Kovler et al., 2004, Xu et al., 1998).

Statistical shape modelling addresses these previous limitations, and has been used to detect subtle changes in bone geometry which could be early predictors of osteoarthritic changes (Bredbenner et al., 2010, Harris et al., 2013, Neogi et al., 2013).

The purpose of this chapter was to firstly, characterise morphological differences between healthy and early osteoarthritic trapezial and first

metacarpal bones. And secondly, to determine the efficacy of using a SSM to detect these early signs of OA through automatic classification of healthy and early osteoarthritic TMC joints.

5.3 Methods
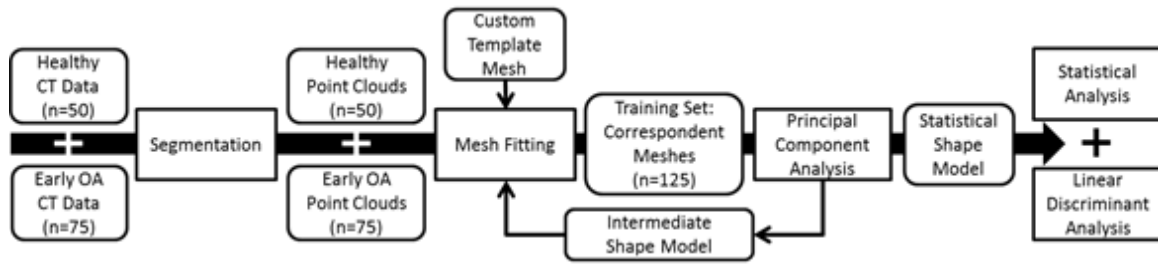
Figure 5.1. Schematic overview of the methods employed in this study.

5.3.1 Subject information and imaging protocol

After Institutional Review Board approval and informed consent, the dominant wrists and thumbs of 50 asymptomatic volunteers (23 men aged 35.6 year ± 13.7 year and 27 women aged 42.9 year ± 15.3 year), and 75 patients with early OA (Eaton stage I, 30 men aged 59.3 year ± 6.5 year and 45 women aged 53.1 year ± 6.0 year), were enrolled as part of a larger study on TMC joint biomechanics (Crisco et al., 2015a, Crisco et al., 2015b, Halilaj et al., 2014a, Halilaj et al., 2014b, Halilaj et al., 2015a, Halilaj et al., 2014c, Halilaj et al., 2015b, Halilaj et al., 2014d, Halilaj et al., 2015c, Schneider et al., 2015). Radiographic inspection of the asymptomatic subjects was performed by a board certified orthopaedic hand surgeon to rule out prior conditions that may affect the study. Inclusion criteria for OA included pain without gross radiographic changes. All subjects were imaged with a 16-slice clinical CT scanner (GE LightSpeed 16, General Electric, Milwaukee, WI) with the following scanner settings: tube parameters at 80 kVp and 80 mA, slice

thickness of 0.625 mm, and in-plane resolution of at least 0.4 mm × 0.4 mm. Subjects were imaged in clinical neutral positions standardised with a custom wrist and thumb spica-splint brace (Rolyan Original, Patterson Medical, Bolingbrook, IL).

5.3.2 Statistical shape model generation

Methods from a previous study were used to generate our SSM (Schneider et al., 2015). Briefly, the trapezia and the first metacarpals were segmented semi-automatically using Mimics v12.11 (Materialise, Leuven, Belgium) and 3-D bone models were exported as meshed surfaces. The vertices of these surfaces were extracted to produce a training set of point clouds (Figure 5.1).

A custom template mesh consisting of cubic-Lagrange piece-wise elements (Nielsen, 1987) was designed to parameterise the first metacarpal and trapezial bones. This parametric template mesh was fitted to all point clouds in the training set via an iterative fitting process that produced maximally correspondent meshes (Figure 5.1). The process involved a series of coarse to fine fits that followed initial rigid alignment to the data clouds. Fitted meshes were then rigidly aligned to each other by minimising the least squared distances of corresponding points. This was followed with a PCA on the mesh node coordinates of the correspondent meshes to obtain a SSM (Figure 5.1). This process was repeated five times, during which the shape model was first used to fit the mesh, thereby propagating fitting correspondence across the training set. This resulted in maximally correspondent meshes (Zhang et al., 2014). The final RMS error achieved between each mesh and corresponding data cloud across the training set was 0.39 mm.

5.3.3 Principal component analysis

PCA results in dimensionality reduction and allows any shape x in the training set to be approximated as the sum of the mean shape $\bar{x}$ and the weighted sum of n principal components ϕ (Heimann and Meinzer, 2009, Schneider et al., 2015, Zhang et al., 2014):

$$x = \bar{x} + \sum_{i=0}^{n} \omega_i \phi_i \tag{5.1}$$

where n was chosen such that the accumulated variance explained by the components account for 90 % of the total variation in the population. Thus, the shape of each bone in the training set was described by 10 weights, ω. These weights were used for the following statistical analyses.

5.3.4 Linear discriminant analysis

LDA, a form of supervised learning, was used to classify PC weights of healthy and EOA subjects. LDA is used in machine learning and data analysis to find features that classifies data into distinct groups. This is done by finding the normal to the hyperplane in multidimensional space that best separates the two groups. The data is then projected into the linear subspace consisting of directions which maximise class separation (positive and negative LDA weights) resulting in further dimensionality reduction (Friedman et al., 2001).

5.3.5 Statistical analysis

Q-Q plots and a Shapiro-Wilk test were used to determine normality of the PC weights, and a Levene test was carried out to confirm equal variance to satisfy *t*-test assumptions. *t*-tests with Bonferroni correction were performed for each

principal component to explore shape differences between healthy and osteoarthritic bones. Where significant differences were found, two-way ANOVA was performed to determine interactions between sex and disease state. LDA was performed on the PCA weights to yield LDA weights of healthy and EOA joints. A *t*-test between LDA weights of healthy and EOA joints was performed. Using mean LDA weights for each class, we reconstructed the PCA weights, to recreate the differences between healthy and EOA TMC joints, and calculated the pointwise distance between the two reconstructed joints (Figure 5.4).

5.4 Results

The first ten principal components of the SSM accounted for over 90 % of the total variance in morphology present in the training set (Figure 5.2). The leave-one-out RMS was 0.39 mm. This RMS error was smaller than the voxel dimensions of 0.4 mm × 0.4 mm × 0.6 mm, indicating a representative shape model, and that the size of the training set (n = 125) was sufficiently large. As expected the first principal component was size (Heimann and Meinzer, 2009, Schneider et al., 2015, Zhang et al., 2014) and accounted for 72.7 % of the variation (Figure 5.2). Size did not differ between healthy and early osteoarthritic subjects ($p = 0.463$). A *t*-test between weights of men and women reconfirmed with a larger sample size (Schneider et al., 2015), that men have larger first metacarpals and trapezia than women ($p < 0.001$).
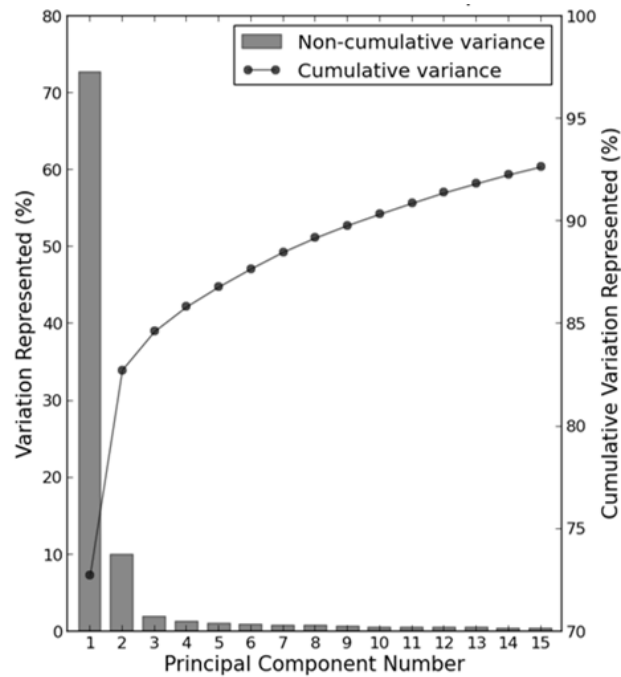
Figure 5.2. Variation and cumulative variation explained by PC modes of the SSM.

After Bonferroni correction, we found that mode 2 and mode 4 were significantly different between early osteoarthritic TMC joint bones and healthy bones (Figure 5.3). Two-way ANOVA between sex and disease state for mode 2 determined that sex and diseased state each had a significant effect on the weights for mode 2 ($p < 0.001$), but no interaction was present between sex and disease state ($p = 0.51$). No interaction was found between sex and disease state for mode 4 ($p = 0.2$).

Mode 2 described 10 % of the morphological variability in the population, and manifested partly as variation in aspect ratio (height to width ratio) for the first metacarpal and trapezial bones. Early osteoarthritic metacarpals exhibited a smaller aspect ratio (shorter and wider) than healthy metacarpals ($p = 0.002$), which exhibited a higher aspect ratio (longer and narrower). In the trapezium, this mode also determined the degree of degradation of the articular surface as seen with a wider articular surface (radial-ulnarly) and deeper groove in early osteoarthritic trapezia (Figure 5.3).
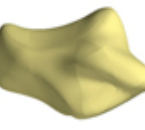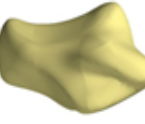
	$\bar{x} + 2\sigma$ (EOA)	$\bar{x}$	$\bar{x} - 2\sigma$ (Healthy)	$p - value$
Mode 2				0.00236
Mode 4				0.0303

Figure 5.3. PC weights between early osteoarthritic (EOA) (+ 2 σ) and healthy TMC joints (− 2 σ) were different in modes 2 and 4 (p < 0.05).

Mode 4 accounted for 1.2 % of the total variance, and partly manifested as the radius of the proximal metaphysis in the first metacarpal. Early osteoarthritic metacarpals have an hourglass profile along the diaphysis, with wider ends meeting at a narrower proximal metaphysis ($p = 0.03$ after Bonferroni correction). This was compared with a straighter profile in the healthy

metacarpals. Mode 4 also accounted for a protrusion at the base of the volar side of the first metacarpal in early osteoarthritic metacarpals. In the trapezium, mode 4 also accounted for the angle of the tangent of the radial surface, to the ulnar-radial axis. In early osteoarthritic trapezia ($+ 2\sigma$), this angle was more acute, compared with healthy trapezia ($- 2\sigma$), where the angle was more obtuse.
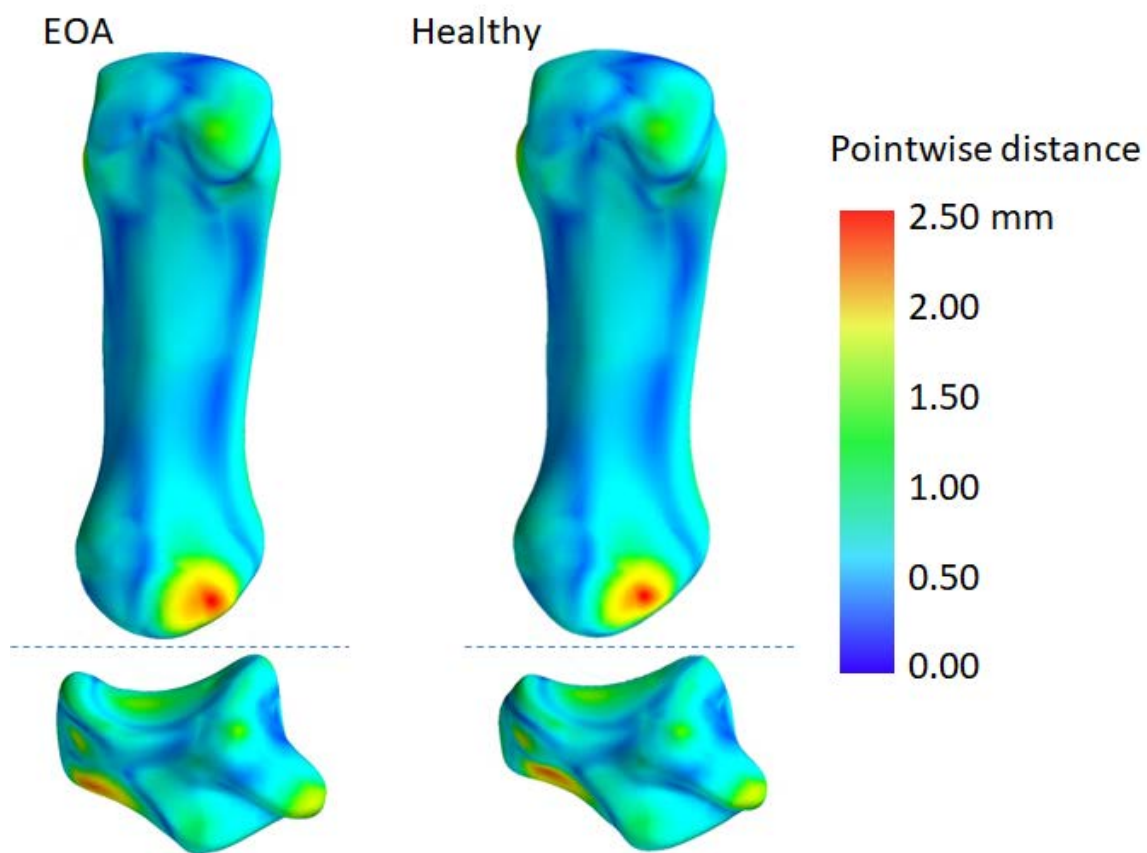
Figure 5.4. Absolute pointwise distance between LDA based reconstructions of early osteoarthritic (EOA) TMC bones against healthy, non-osteoarthritic TMC bones.

A quantitative pointwise distance plot, between TMC joints reconstructed from mean LDA weights for each class indicates regions that differ up to 2.5 mm (Figure 5.4). The articular surfaces were on average 1.0 mm to 1.5 mm deeper in the early osteoarthritic trapezia than in healthy trapezia, and the radial and ulnar ridges of early osteoarthritic trapezia were 1.5 mm higher than in healthy trapezia. These ridges correspond to bone growth around the articular surface. The average difference in protrusion size on the volar beak of the first metacarpal was 2.5 mm, and 2.5 mm at the trapezoid facet.

The LDA score for classifying datasets within the training set was 0.78 when 11 modes were included (Figure 5.5), meaning that 78 % of all data were correctly classified. The model achieved a sensitivity of 82.7 % and specificity of 71.4 %. The leave-one-out analysis showed that the accuracy of the model when classifying new data was 73.6 % (Table 5.1). The LDA model was able to classify a significant difference between early osteoarthritic and healthy subjects with just the inclusion of two PC modes ($p = 0.0015$). The level of significance increased greatly with the inclusion of more modes in the LDA model ($p < 0.001$ at the inclusion of 4 modes).

Table 5.1. Leave-one-out confusion matrix for LDA classifier. Performance metrics: Accuracy: 73.6 %; Error rate: 26.4 %; Sensitivity (true positive rate): 77.3 %; False positive rate: 32.0 %; Specificity: 68.0 %; Precision (positive predictive value): 78.4 %.

		Predicted		
		Healthy	Early OA	
Actual	Healthy	34	16	50
	Early OA	17	58	75
		51	74	
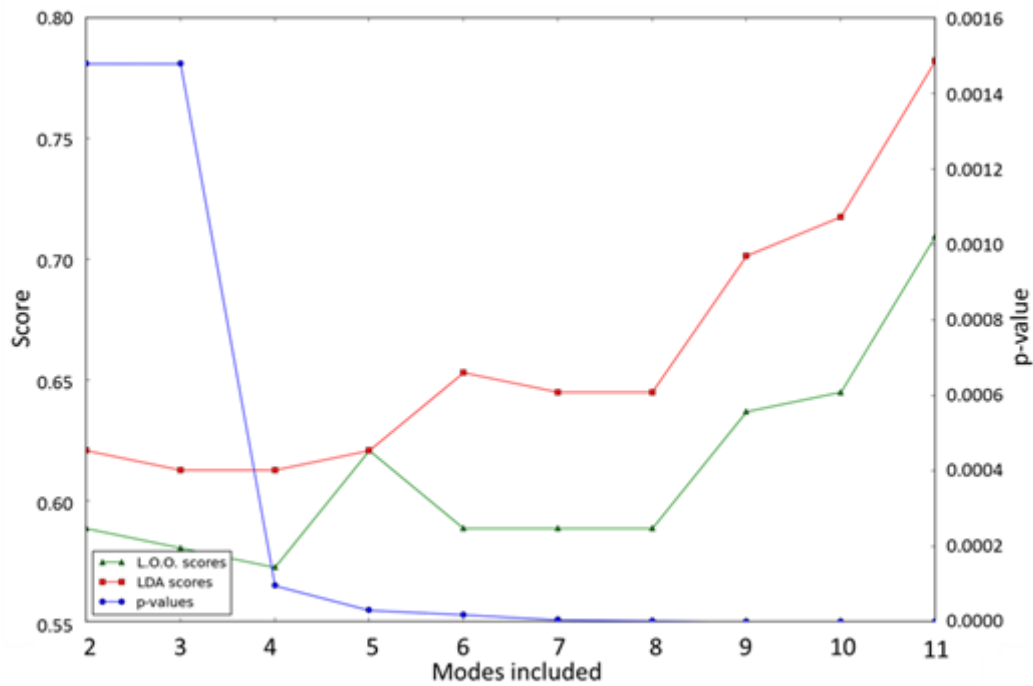
Figure 5.5. LDA model performance; few modes were required by the LDA model to classify a significant difference between healthy and early osteoarthritic TMC joints. However, the inclusion of more modes increased the classification accuracy. Leave-one-out (L.O.O.) scores indicate the accuracy when classifying new data that were not part of the training set either as early osteoarthritic or healthy. LDA scores indicate the accuracy when classifying data that were included within the training set. P-values indicate how significant the differences were between the LDA weights of early osteoarthritic and healthy subjects for the number of modes included in the LDA model.

5.5 Discussion

The purpose of this chapter was to characterise morphological differences between healthy and early osteoarthritic trapezial and first metacarpal bones, and to determine the efficacy of using a SSM to detect subtle signs of OA and perform automatic classification of healthy and early osteoarthritic TMC joints. Statistical shape modelling alone was able to describe morphological variability of both healthy and early osteoarthritic data efficiently (90 % variability with 10 modes) and accurately (RMS = 0.39 mm). We determined two modes of shape variation that were present between healthy and early osteoarthritic TMC joint bones (Figure 5.3). Combining shape modelling with LDA allowed the visualisation of the average shape differences in two LDA reconstructed models (Figure 5.4). Lastly, automated classification of healthy and early osteoarthritic TMC joints displayed promise for early identification of TMC joint OA.

TMC joint bones of early osteoarthritic subjects exhibited a lower aspect ratio compared with healthy subjects (Figure 5.3). This variation may play a role in the development of OA of the TMC joint (Kovler et al., 2004, Schneider et al., 2015, Xu et al., 1998). Xu et al. (1998) rationalised that smaller joints would experience higher stresses because smaller bones have smaller contact areas, and because activities of daily living required similar loads. Opening a jar, for example, demands a fixed torque, regardless of joint size. Since aspect ratio directly affects the size of muscle moment arms crossing the joint, a joint with lower aspect ratio would require a larger force to generate the same torque due to a smaller moment arm, when compared to a joint with higher aspect ratio. As cartilage responds to the load history, we hypothesise that this morphology may place the joint at an increased risk of acute stress that may promote cartilage degeneration.

We found protrusions (mean size = 2.5 mm) at the volar beak of the first metacarpal (Figure 5.4). Degeneration in this area has been previously reported

(Doerschuk et al., 1999, Pellegrini, 1991), and believed to be a result of volar beak ligament degeneration. Early osteoarthritic trapezia displayed widening of the articular surface in the radio-ulnar axis, deepening of the subchondral articular surface, as well as protruding bone growths (likely early osteophytes) along the concave margin (Figure 5.3), similar to those reported by Kovler et al. (2004). This change in the height to width ratio of the trapezium supports the thumb OA index as a measure for grading osteoarthritic stage (Ladd et al., 2015). Unlike aspect ratio, these morphological differences do not appear to be the cause of OA, but instead liken to early stage OA symptoms (Kovler et al., 2004, North and Rutledge, 1983) and instead are likely to be a consequence of degeneration. Studies have reported cartilage degeneration in different portions of facets of the trapezium at different stages of the disease. Koff et al. (2003) reported cartilage thinning in the radial and volar quadrants in early OA. In later OA, Van Nortwick et al. (2013) stated that three disparate patterns of trapezial degeneration exist in the bone (saddle, dish and cirque), but was uncertain if one may progress more rapidly to the other. Kovler et al. (2004) hypothesised that the radial region might be affected early on with the volar region being affected later on in the disease due to a shift in biomechanics resulting from changes in joint shape. On the contrary, our findings suggest that degenerative changes in the subchondral bone of early osteoarthritic trapezium occur throughout the articular surface and are not contained to a single quadrant (Figure 5.4). Furthermore, our findings indicate that osteoarthritic degeneration is well underway in the early stage, with potential osteophytic growths already becoming detectable by our LDA shape model.

The trapezoid-facet of the trapezium displayed a protrusion (up to 2.5 mm) in early osteoarthritic subjects (Figure 5.4). It is unclear if this protrusion is an osteophytic growth or merely a morphological risk factor of TMC joint OA, and appears to be a new finding. This contrasts with the report by North and Eaton (1983) that degenerative changes were rare in the trapezium-trapezoid

joint. Cooney and Chao (1977) showed that forces at the base of the thumb can be as high as 12 times the applied load at the tip of the thumb, with up to 1.2 kN compressive force generated across the TMC joint during grasp. We speculate that the trapezium-trapezoidal joint may also experience these high loads, especially during jar twist, and may be susceptible to acute loads and stresses on the trapezoid-facet.

Statistical shape modelling combined with LDA and point-wise distance mapping (Figure 5.4) provided a visual presentation of the mean differences between healthy and osteoarthritic TMC joint bones across a large population (n = 125). Local morphology varied by as much as 2.5 mm (Figure 5.4), but also subtle morphological changes (< 1 mm), which might not be detected in a radiograph by a clinician, were detected by the shape model. The differences found were subtle, which lends support to the theory that the degenerative process is already underway, and that any morphological changes (such as radiographic signs in joint space narrowing) should be considered as symptoms of a late stage of the disease rather than early (Xu et al., 1998). Based on these differences, LDA based automatic classification of healthy and early osteoarthritic TMC joints achieved a sensitivity of 82.7 % and a specificity of 71.4 %. This method shows promise for determining the risk of OA development early and automatically (Figure 5.5). With the inclusion of more data, including mid-stage to late-stage osteoarthritic subjects, we can characterise the natural history of the disease leading to a more complete understanding of the pathogenesis of TMC OA.

Our study is not without its limitations. The study was not longitudinal, and therefore we were unable to track the onset of OA, or determine a causal relationship. A second limitation was that we were unable to analyse the cartilage, since clinical CT without contrast agents is unable to detect cartilage. High resolution MRI data combined with this pipeline would provide more information with regards to cartilage thickness, and would remove the exposure

of the subjects to harmful radiation from CT scanning. Further work in this field should include longitudinal analysis of shape change with disease progression to determine the progression of the disease, longitudinal tracking of healthy TMC joints to determine which parameters play a role in the onset of OA, and cartilage imaging.

This study has shown that differences in morphology to healthy TMC joint bones are already present in early osteoarthritic TMC joint bones and can be detected by SSMs. The application of SSMs with MRI data shows promise for a clinical tool that can automatically perform early detection and staging of TMC joint OA. Further work needs to be performed with longitudinal data to determine the value of shape models as clinical diagnosis or staging tools.

Chapter 6.

Conclusions and future directions

The aim of this thesis was to progress our understanding of the onset and development of TMC joint OA from a biomechanical point of view. To that end, we created a computational framework for investigating the relationship between TMC morphology, kinematics, and cartilage stress distributions in men and women.

To achieve our aim, we first developed a SSM of the TMC joint bones, and used it to create an automatic 3D segmentation tool for the TMC joint (Chapter 2). Next, we used the shape model to characterise the healthy three-dimensional morphology as a function of sex and age (Chapter 3). This was followed with the development of a parametric population FE model of the TMC joint, which we used to classify the cartilage stress distributions as a function of sex, age, and task (Chapter 4). Finally, we created a shape model classifier of healthy and early OA subjects to investigate shape differences between healthy and early OA TMC joints, and tested the efficacy of the classifier as a clinical tool for detecting early morphologic changes in OA (Chapter 5).

The preceding chapters include detailed discussions and results of each of the studies in this thesis (Chapters 3 to 5). The following chapter briefly

summarises the main conclusions of those studies and discusses potential future work.

6.1 Morphology of healthy TMC joint bones

In Chapter 3, we characterised the healthy three-dimensional morphology of the TMC joint bones as a function of sex and age in a cohort of 50 healthy subjects. To achieve this, we developed two SSMs, size-normalised and non size-normalised models, of the trapezial and first metacarpal bones with a training set of 50 CT images of the wrist. This was followed with statistical investigation of the effects of sex and age on the size and shape of the TMC joint bones as well as the articulating surface areas. In our analysis, we observed sex differences in morphology that manifested as bone size, which accounted for over 70 % of the variance in morphology. However, we were unable to detect any shape differences that were linked to age, and found age to be a poor predictor of morphology. As expected, we found the same trends in the articular surfaces, which supported the hypothesis that smaller joints in women may experience higher stresses than the larger joints in men due to smaller articular surfaces and similar loads during activities of daily living. Our findings also suggested that size itself could be an important factor that is often overlooked. Size is especially important when considering the biomechanics of the joint, specifically the forces experienced in the joint during activities of daily living, such as grasping a door handle and opening a jar. Scaling of the bone influences the action of ligaments, muscles, and the size of the moment arms of muscle crossing the joint. The variation in size may place certain individuals at an increased risk of developing TMC OA. Furthermore, our findings have implications that extend to TMC joint implant design and scaling of musculoskeletal models for the investigation of TMC joint function.

6.2 Healthy TMC joint contact stress distributions

In Chapter 4, we developed a parametric population FE model of the TMC joint and used it to characterise healthy cartilage stress distributions as a function of sex, age, and task. In particular, we investigated the sex and age differences in contact area and peak stress location of the TMC joint during three isometric tasks including pinch, grasp, and jar twist in a cohort of 50 healthy subjects. Statistical methods of analyses such as PCA, linear regression, and LDA were performed to test for sex and age differences in the SED distribution. We found no sex or age differences in contact area but observed sex differences in peak stress locations and the SED distribution during all three tasks. Furthermore, age was also a poor predictor of peak stress location. Parametric modelling allowed the comparison of FE simulation results in the same frame of reference and greatly improved the visualisation of our findings, which show that the apparent natural variation in peak stress location is higher in women during grasp and jar twist tasks than in men. We found that jar twist consistently resulted in peak stresses located in the central-radial region when performed by men, but produced variably located peak stresses in women. This suggests higher variability in how these tasks are performed among women which might play a role in the increased incidence of OA in women. We found that a subset of both men and women exhibited peak cartilage stresses in regions where degenerative changes are frequently observed, supporting the hypothesis that cartilage degeneration may occur through divergent mechanisms rather than a single progression pattern. This work advances our understanding of healthy TMC biomechanics that is essential to the understanding of joint pathology, and has further implications in musculoskeletal modelling of TMC joint contact.

6.3   Early morphologic changes in TMC OA

In Chapter 5, we characterised the morphological differences between healthy and early osteoarthritic TMC joints, and created a classifier to detect these differences in a cohort of 125 subjects. Using a CT data from of 50 healthy subjects and 75 subjects with early OA, we created a SSM of the healthy and early osteoarthritic TMC joint bones. A linear discriminant classifier was trained on the PC weights, and leave one out classification was performed to characterise features of each group and evaluate the ability of the classifier to detect signs of early OA. We found that lower aspect ratio correlated to early OA in the TMC joint, which lends support to the hypothesis that joint with shorter muscle moment arms may be at an increased risk of acute stressing that may promote cartilage degeneration. We found protrusions at the volar beak, widening and deepening of the articular surface, as well as osteophytes along the concave margin, which support the use of the thumb OA index as a measure for grading OA severity, and which may suggest that OA is more a disease of the bone rather than cartilage. Combining shape modelling with LDA enabled better visual presentation of average shape differences between the two groups, which suggested that degenerative changes in the subchondral bone of early OA trapezia are not constrained to a single quadrant, but instead occur throughout the articular surface. Automated classification produced a sensitivity of 82.7 % and specificity of 71.4%, showing promise for a potential clinical tool that combines shape models with MRI for the purpose of early identification of TMC joint OA. The implications of this work are important for understanding OA pathology and for early detection that allows better treatment and disease management.

6.4 Future directions

In reflecting on the research completed in this thesis, we observed several avenues of future work that would expand on the findings of this thesis.

A major challenge of this thesis was the limited data on TMC joint cartilage in the literature in terms of material properties and morphology. For the material properties, we assumed that cartilage properties were similar across joints, and were used material properties from the ankle, hip, knee, and shoulder cartilage. However, the morphology of both healthy and osteoarthritic TMC joint cartilage is an area of research that requires more energy. Future work should be directed towards *in vivo* collection of high resolution 3D cartilage data through means such as MRI and spectral molecular imaging, or *ex vivo* collection of morphology data of TMC cartilage from fresh cadavers through micro CT or laser scanning. Material property testing of TMC joint cartilage should also be carried out, as cartilage properties are known to vary in different joints as well as within the same joint (Sophia Fox et al., 2009). Together, this data would allow for the study of cartilage morphology and its relationship to regional variation in material properties, and enable the creation of more accurate computational models for the analysis of stress and strain the TMC joint. These models are important for understanding the aetiology of TMC joint OA.

There is growing evidence that neuromuscular control is responsible for the stability of the TMC joint, and that loss of this control plays a role in OA pathogenesis. Understanding the muscle forces and coordination of muscles involved in thumb manipulation remains an area of research that is currently still premature. Despite limited data in the literature on thumb muscle forces, we could depend on force vector optimisation in our population FE model (Chapter 4). However, this process is computationally expensive. Ideally, such an FE model would incorporate true muscle force data combined with 3D

muscle models. Therefore, future work should be directed at collecting hand muscle morphology and force data for the purpose of creating realistic 3D biomechanical muscle models.

In this thesis, we examined relationships between morphology and patient demographics such as sex and age, in healthy and early osteoarthritic TMC joints. Further analysis of morphology is warranted and should be directed towards characterising the progression of osteoarthritic morphology in the TMC joint from early to late stage OA. This research will require an exploration of methods to quantify osteophytic growths and accommodate for complex geometries that result from pathology. Ideally, high resolution longitudinal data are collected for this analysis. This can be coupled with longitudinal kinematics data from early to late stage OA, to investigate the expected changes in kinematics from a change in morphology. This work is important for understanding TMC joint OA progression and may shed light on the aetiology of OA.

Understanding the onset of OA continues to be a challenge that the community faces. Abnormal joint stress and strain are implicated at the pathogenesis of OA, and remains to be the prevailing explanation for its onset in the TMC joint. Although we have characterised the stress and strain the TMC joint in Chapter 4, ideally, this work should be repeated with patient specific cartilage models, using cartilage material properties, muscle models, and muscle force data obtained from experimental measurements, with subjects performing a range of tasks. A more complete population FE model will enable us to correlate kinematics to stress distributions. We can perform this analysis on early OA data to investigate what abnormal TMC joint stress and strain looks like. Furthermore, data should be collected longitudinally, such that we can track subjects that develop OA and pinpoint the causes of OA onset.

Bibliography

Acheson, R., Chan, Y.-K. & Clemett, A. 1970. New Haven survey of joint diseases. XII. Distribution and symptoms of osteoarthrosis in the hands with reference to handedness. *Annals of the rheumatic diseases,* 29**,** 275.

Anderson, A. E., Ellis, B. J., Maas, S. A., Peters, C. L. & Weiss, J. A. 2008. Validation of finite element predictions of cartilage contact pressure in the human hip joint. *Journal of biomechanical engineering,* 130**,** 051008.

Anderson, A. E., Ellis, B. J., Maas, S. A. & Weiss, J. A. 2010. Effects of idealized joint geometry on finite element predictions of cartilage contact stresses in the hip. *Journal of biomechanics,* 43**,** 1351-1357.

Anderson, D. D., Goldsworthy, J. K., Li, W., Rudert, M. J., Tochigi, Y. & Brown, T. D. 2007. Physical validation of a patient-specific contact finite element model of the ankle. *Journal of biomechanics,* 40**,** 1662-1669.

Armstrong, A., Hunter, J. & Davis, T. 1994. The prevalence of degenerative arthritis of the base of the thumb in post-menopausal women. *Journal of Hand Surgery,* 19**,** 340-341.

Arnold, A. S. & Delp, S. L. 2001. Rotational moment arms of the medial hamstrings and adductors vary with femoral geometry and limb position: implications for the treatment of internally rotated gait. *Journal of biomechanics,* 34**,** 437-447.

Ateshian, G., Rosenwasser, M. & Mow, V. 1992. Curvature characteristics and congruence of the thumb carpometacarpal joint: differences between female and male joints. *Journal of biomechanics,* 25**,** 591-607.

Ateshian, G. A., Ark, J. W., Rosenwasser, M. P., Pawluk, R. J., Soslowsky, L. J. & Mow, V. C. 1995. Contact areas in the thumb carpometacarpal joint. *Journal of Orthopaedic Research,* 13**,** 450-458.

Ateshian, G. A., Ellis, B. J. & Weiss, J. A. 2007. Equivalence between short-time biphasic and incompressible elastic material responses. *Journal of biomechanical engineering,* 129**,** 405-412.

Baker-Lepain, J. C. & Lane, N. E. 2010. Relationship between joint shape and the development of osteoarthritis. *Current opinion in rheumatology,* 22**,** 538.

Batra, S. & Kanvinde, R. 2007. Osteoarthritis of the thumb trapeziometacarpal joint. *Current Orthopaedics,* 21**,** 135-144.

Beck, M., Kalhor, M., Leunig, M. & Ganz, R. 2005. Hip morphology influences the pattern of damage to the acetabular cartilage. *Bone & Joint Journal,* 87**,** 1012-1018.

Bettinger, P. C., Linscheid, R. L., Berger, R. A., Cooney, W. P. & An, K.-N. 1999. An anatomic study of the stabilizing ligaments of the trapezium and trapeziometacarpal joint. *The Journal of hand surgery,* 24**,** 786-798.

Bettinger, P. C., Smutz, W. P., Linscheid, R. L., Cooney, W. P. & An, K.-N. 2000. Material properties of the trapezial and trapeziometacarpal ligaments. *The Journal of hand surgery,* 25**,** 1085-1095.

Bischoff, J. E., Dai, Y., Goodlett, C., Davis, B. & Bandi, M. 2014. Incorporating population-level variability in orthopedic biomechanical analysis: a review. *Journal of biomechanical engineering,* 136**,** 021004.

Blankevoort, L., Kuiper, J., Huiskes, R. & Grootenboer, H. 1991. Articular contact in a three-dimensional model of the knee. *Journal of biomechanics,* 24**,** 1019-1031.

Bredbenner, T. L., Eliason, T. D., Potter, R. S., Mason, R. L., Havill, L. M. & Nicolella, D. P. 2010. Statistical shape modeling describes variation in tibia and femur surface geometry between Control and Incidence groups from the osteoarthritis initiative database. *Journal of biomechanics,* 43**,** 1780-1786.

Brunelli, G. & Brunelli, G. Anatomical study of distal insertion of the abductor pollicis longus concept of a new musculo-tendinous unit: the abductor carpi muscle. Annales de Chirurgie de la Main et du Membre Superieur, 1991. Elsevier, 569-576.

Büchler, P., Ramaniraka, N., Rakotomanana, L., Iannotti, J. & Farron, A. 2002. A finite element model of the shoulder: application to the comparison of normal and osteoarthritic joints. *Clinical Biomechanics,* 17**,** 630-639.

Butz, K. D., Chan, D. D., Nauman, E. A. & Neu, C. P. 2011. Stress distributions and material properties determined in articular cartilage from MRI-based finite strains. *Journal of biomechanics,* 44**,** 2667-2672.

Carter, D. R., Beaupré, G. S., Wong, M., Smith, R. L., Andriacchi, T. P. & Schurman, D. J. 2004. The mechanobiology of articular cartilage development and degeneration. *Clinical orthopaedics and related research,* 427**,** S69-S77.

Chan, E. F., Farnsworth, C. L., Koziol, J. A., Hosalkar, H. S. & Sah, R. L. 2013. Statistical shape modeling of proximal femoral shape deformities in Legg–Calvé–Perthes disease and slipped capital femoral epiphysis. *Osteoarthritis and cartilage,* 21**,** 443-449.

Conconi, M., Halilaj, E., Castelli, V. P. & Crisco, J. J. 2014. Is early osteoarthritis associated with differences in joint congruence? *Journal of biomechanics,* 47**,** 3787-3793.

Cooney, W. P. & Chao, E. 1977. Biomechanical analysis of static forces in the thumb during hand function. *J Bone Joint Surg Am,* 59**,** 27-36.

Cootes, T. F., Cooper, D. H., Taylor, C. J. & Graham, J. 1992. Trainable method of parametric shape description. *Image and Vision Computing,* 10**,** 289-294.

Cootes, T. F., Ionita, M. C., Lindner, C. & Sauer, P. Robust and accurate shape model fitting using random forest regression voting. European Conference on Computer Vision, 2012. Springer, 278-291.

Crisco, J. J., Coburn, J. C., Moore, D. C. & Upal, M. A. 2005. Carpal bone size and scaling in men versus in women. *The Journal of hand surgery,* 30**,** 35-42.

Crisco, J. J., Halilaj, E., Moore, D. C., Patel, T., Weiss, A.-P. C. & Ladd, A. L. 2015a. In vivo kinematics of the trapeziometacarpal joint during thumb extension-flexion and abduction-adduction. *The Journal of hand surgery,* 40**,** 289-296.

Crisco, J. J., Patel, T., Halilaj, E. & Moore, D. C. 2015b. The envelope of physiological motion of the first carpometacarpal joint. *Journal of biomechanical engineering,* 137**,** 101002.

De Monsabert, B. G., Vigouroux, L., Bendahan, D. & Berton, E. 2014. Quantification of finger joint loadings using musculoskeletal modelling clarifies mechanical risk factors of hand osteoarthritis. *Medical engineering & physics,* 36**,** 177-184.

Dias, R., Chandrasenan, J., Rajaratnam, V. & Burke, F. D. 2007. Basal thumb arthritis. *Postgraduate medical journal,* 83**,** 40-43.

Dingle, J. T. 1981. Catabolin-A Cartilage Catabolic Factor from Synovium. *Clinical orthopaedics and related research,* 156**,** 219-231.

Doerschuk, S. H., Hicks, D. G., Chinchilli, V. M. & Pellegrini, V. D. 1999. Histopathology of the palmar beak ligament in trapeziometacarpal osteoarthritis. *The Journal of hand surgery,* 24**,** 496-504.

Dryden, I. L. & Mardia, K. V. 1998. Statistical shape analysis.

Eaton, R. G. & Littler, J. W. 1969. A Study of the Basal Joint of the Thumb: Treatment of its Disabilities by Fusion. *JBJS,* 51**,** 661-668.

Eaton, R. G. & Littler, J. W. 1973. Ligament reconstruction for the painful thumb carpometacarpal joint. *J Bone Joint Surg Am,* 55**,** 1655-1666.

Edmunds, J. O. 2011. Current concepts of the anatomy of the thumb trapeziometacarpal joint. *The Journal of hand surgery,* 36**,** 170-182.

Ferguson, S., Bryant, J. T., Ganz, R. & Ito, K. 2003. An in vitro investigation of the acetabular labral seal in hip joint mechanics. *Journal of biomechanics,* 36**,** 171-178.

Fitzpatrick, C. K., Baldwin, M. A., Laz, P. J., Fitzpatrick, D. P., Lerner, A. L. & Rullkoetter, P. J. 2011. Development of a statistical shape model of the patellofemoral joint for investigating relationships between shape and function. *Journal of biomechanics,* 44**,** 2446-2452.

Friedman, J., Hastie, T. & Tibshirani, R. 2001. *The elements of statistical learning,* Springer series in statistics Springer, Berlin.

Giurintano, D., Hollister, A., Buford, W., Thompson, D. & Myers, L. 1995. A virtual five-link model of the thumb. *Medical engineering & physics,* 17**,** 297-303.

Gray, H. 1918. *Anatomy of the human body,* Philadelphia, Lea & Febiger.

Haara, M. M., Heliövaara, M., Kröger, H., Arokoski, J. P., Manninen, P., Kärkkäinen, A., Knekt, P., Impivaara, O. & Aromaa, A. 2004. Osteoarthritis in the carpometacarpal joint of the thumb. *J Bone Joint Surg Am,* 86**,** 1452-1457.

Hadid, A., Epstein, Y., Shabshin, N. & Gefen, A. 2012. Modeling mechanical strains and stresses in soft tissues of the shoulder during load carriage based on load-bearing open MRI. *Journal of Applied Physiology,* 112**,** 597-606.

Halilaj, E., Laidlaw, D. H., Moore, D. C. & Crisco, J. J. 2014a. How do sex, age, and osteoarthritis affect cartilage thickness at the thumb carpometacarpal joint? insights from subject-specific cartilage modeling. *Bio-Imaging and Visualization for Patient-Customized Simulations.* Springer.

Halilaj, E., Moore, D. C., Laidlaw, D. H., Got, C. J., Weiss, A.-P. C., Ladd, A. L. & Crisco, J. J. 2014b. The morphology of the thumb carpometacarpal joint does not differ between men and women, but changes with aging and early osteoarthritis. *Journal of biomechanics,* 47**,** 2709-2714.

Halilaj, E., Moore, D. C., Patel, T. K., Ladd, A. L., Weiss, A. P. C. & Crisco, J. J. 2015a. Early osteoarthritis of the trapeziometacarpal joint is not associated with joint instability during typical isometric loading. *Journal of Orthopaedic Research,* 33**,** 1639-1645.

Halilaj, E., Moore, D. C., Patel, T. K., Laidlaw, D. H., Ladd, A. L., Weiss, A.-P. C. & Crisco, J. J. Thumb carpometacarpal joint congruence during functional tasks and thumb range-of-motion activities. Engineering in Medicine and Biology Society (EMBC), 2014 36th Annual International Conference of the IEEE, 2014c. IEEE, 4354-4357.

Halilaj, E., Moore, D. C., Patel, T. K., Laidlaw, D. H., Ladd, A. L., Weiss, A.-P. C. & Crisco, J. J. 2015b. Older asymptomatic women exhibit patterns of thumb carpometacarpal joint space narrowing that precede changes associated with early osteoarthritis. *Journal of biomechanics,* 48**,** 3634-3640.

Halilaj, E., Rainbow, M. J., Got, C., Schwartz, J. B., Moore, D. C., Weiss, A.-P. C., Ladd, A. L. & Crisco, J. J. 2014d. In vivo kinematics of the thumb carpometacarpal joint during three isometric functional tasks. *Clinical Orthopaedics and Related Research®,* 472**,** 1114-1122.

Halilaj, E., Rainbow, M. J., Moore, D. C., Laidlaw, D. H., Weiss, A.-P. C., Ladd, A. L. & Crisco, J. J. 2015c. In vivo recruitment patterns in the anterior oblique and dorsoradial ligaments of the first carpometacarpal joint. *Journal of biomechanics,* 48**,** 1893-1898.

Harris, M. D., Datar, M., Whitaker, R. T., Jurrus, E. R., Peters, C. L. & Anderson, A. E. 2013. Statistical shape modeling of cam femoroacetabular impingement. *Journal of Orthopaedic Research,* 31**,** 1620-1626.

Heimann, T. & Meinzer, H.-P. 2009. Statistical shape models for 3D medical image segmentation: a review. *Medical image analysis,* 13**,** 543-563.

Hollister, A., Buford, W. L., Myers, L. M., Giurintano, D. J. & Novick, A. 1992. The axes of rotation of the thumb carpometacarpal joint. *Journal of Orthopaedic Research,* 10**,** 454-460.

Hunter, D., Zhang, Y., Sokolove, J., Niu, J., Aliabadi, P. & Felson, D. 2005. Trapeziometacarpal subluxation predisposes to incident trapeziometacarpal osteoarthritis (OA): the Framingham Study. *Osteoarthritis and cartilage,* 13**,** 953-957.

Hunter, D. J. & Wilson, D. R. 2009. Role of alignment and biomechanics in osteoarthritis and implications for imaging. *Radiologic Clinics of North America,* 47**,** 553-566.

Katz, S., Downs, T. D., Cash, H. R. & Grotz, R. C. 1970. Progress in development of the index of ADL. *The gerontologist,* 10**,** 20-30.

Kempson, G. E. 1980. The mechanical properties of articular cartilage. *The joints and synovial fluid,* 2**,** 177-238.

Kim, W., Hutchinson, C., Andrew, J. & Allen, P. 2006. The relationship between acetabular retroversion and osteoarthritis of the hip. *Bone & Joint Journal,* 88**,** 727-729.

Koff, M. F., Ugwonali, O. F., Strauch, R. J., Rosenwasser, M. P., Ateshian, G. A. & Mow, V. C. 2003. Sequential wear patterns of the articular cartilage of the thumb carpometacarpal joint in osteoarthritis. *The Journal of hand surgery,* 28**,** 597-604.

Kovler, M., Lundon, K., Mckee, N. & Agur, A. 2004. The human first carpometacarpal joint: osteoarthritic degeneration and 3-dimensional modeling. *Journal of Hand Therapy,* 17**,** 393-400.

Kuczynski, K. 1974. Carpometacarpal joint of the human thumb. *Journal of Anatomy,* 118**,** 119.

Ladd, A. L., Crisco, J. J., Hagert, E., Rose, J. & Weiss, A.-P. C. 2014. The 2014 ABJS Nicolas Andry Award: The Puzzle of the Thumb: Mobility, Stability, and Demands in Opposition. *Clinical Orthopaedics and Related Research®,* 472**,** 3605-3622.

Ladd, A. L., Messana, J. M., Berger, A. J. & Weiss, A.-P. C. 2015. Correlation of clinical disease severity to radiographic thumb osteoarthritis index. *The Journal of hand surgery,* 40**,** 474-482.

Ladd, A. L., Weiss, A.-P. C., Crisco, J. J., Hagert, E., Wolf, J. M., Glickel, S. Z. & Yao, J. 2013. The thumb carpometacarpal joint: anatomy, hormones, and biomechanics. *Instructional course lectures,* 62**,** 165.

Lindner, C., Thiagarajah, S., Wilkinson, J., Consortium, T., Wallis, G. & Cootes, T. 2013. Fully automatic segmentation of the proximal femur using random forest regression voting. *IEEE transactions on medical imaging,* 32**,** 1462-1472.

Maas, S. A., Ellis, B. J., Ateshian, G. A. & Weiss, J. A. 2012. FEBio: finite elements for biomechanics. *J Biomech Eng,* 134**,** 011005.

Macirowski, T., Tepic, S. & Mann, R. 1994. Cartilage stresses in the human hip joint. *Transactions-American Society of Mechanical Engineers Journal of Biomechanical Engineering,* 116**,** 10-10.

Marzke, M. W., Tocheri, M. W., Marzke, R. F. & Femiani, J. D. 2012. Three-dimensional quantitative comparative analysis of trapezial-metacarpal joint surface curvatures in human populations. *The Journal of hand surgery,* 37**,** 72-76.

Momose, T., Nakatsuchi, Y. & Saitoh, S. 1999. Contact area of the trapeziometacarpal joint. *The Journal of hand surgery,* 24**,** 491-495.

Moore, D. C., Crisco, J. J., Trafton, T. G. & Leventhal, E. L. 2007. A digital database of wrist bone anatomy and carpal kinematics. *Journal of biomechanics,* 40**,** 2537-2542.

Najima, H., Oberlin, C., Alnot, J. & Cadot, B. 1997. Anatomical and biomechanical studies of the pathogenesis of trapeziometacarpal degenerative arthritis. *The Journal of Hand Surgery: British & European Volume,* 22**,** 183-188.

Nanno, M., Buford, W. L., Patterson, R. M., Andersen, C. R. & Viegas, S. F. 2006. Three-dimensional analysis of the ligamentous attachments of the first carpometacarpal joint. *The Journal of hand surgery,* 31**,** 1160-1170.

Napier, J. 1955. The form and function of the carpo-metacarpal joint of the thumb. *Journal of Anatomy,* 89**,** 362.

Neogi, T., Bowes, M. A., Niu, J., Souza, K. M., Vincent, G. R., Goggins, J., Zhang, Y. & Felson, D. T. 2013. Magnetic resonance imaging–based three‐ dimensional bone shape of the knee predicts onset of knee osteoarthritis: data from the Osteoarthritis Initiative. *Arthritis & Rheumatism,* 65**,** 2048-2058.

Neumann, D. A. 2013. *Kinesiology of the Musculoskeletal System: Foundations for Rehabilitation*, Elsevier Health Sciences.

Nielsen, P. M. F. 1987. *The anatomy of the heart: a finite element model.* ResearchSpace@ Auckland.

Norajitra, T., Meinzer, H.-P. & Maier-Hein, K. H. 3D statistical shape models incorporating 3D random forest regression voting for robust CT liver segmentation. SPIE Medical Imaging, 2015. International Society for Optics and Photonics, 941406-941406-6.

North, E. & Rutledge, W. 1983. The trapezium-thumb metacarpal joint: the relationship of joint shape and degenerative joint disease. *The Hand,* 15**,** 201-206.

North, E. R. & Eaton, R. G. 1983. Degenerative joint disease of the trapezium: a comparative radiographic and anatomic study. *The Journal of hand surgery,* 8**,** 160-167.

Pellegrini Jr, V. D. 2005. The ABJS 2005 Nicolas Andry Award: osteoarthritis and injury at the base of the human thumb: survival of the fittest? *Clinical orthopaedics and related research,* 438**,** 266-276.

Pellegrini, V. D. 1991. Osteoarthritis of the trapeziometacarpal joint: the pathophysiology of articular cartilage degeneration. I. Anatomy and pathology of the aging joint. *The Journal of hand surgery,* 16**,** 967-974.

Pellegrini, V. D., Olcott, C. W. & Hollenberg, G. 1993. Contact patterns in the trapeziometacarpal joint: the role of the palmar beak ligament. *The Journal of hand surgery,* 18**,** 238-244.

Pieron, A. P. 1973. The mechanism of the first carpometacarpal (CMC) joint: an anatomical and mechanical analysis. *Acta Orthopaedica Scandinavica,* 44**,** 1-104.

Qualter, J., Sculli, F., Oliker, A., Napier, Z., Lee, S., Garcia, J., Frenkel, S., Harnik, V. & Triola, M. 2011. The biodigital human: a web-based 3D platform for medical visualization and education. *Studies in health technology and informatics,* 173**,** 359-361.

Ross, A. 2004. Procrustes analysis. *Course report, Department of Computer Science and Engineering, University of South Carolina.*

Schneider, M., Zhang, J., Crisco, J., Weiss, A., Ladd, A., Nielsen, P. & Besier, T. 2015. Men and women have similarly shaped carpometacarpal joint bones. *Journal of biomechanics,* 48**,** 3420-3426.

Segal, R., Avrahami, E., Lebdinski, E., Habut, B., Leibovitz, A., Gil, I., Yaron, M. & Caspi, D. 1998. The impact of hemiparalysis on the expression of osteoarthritis. *Arthritis & Rheumatism,* 41**,** 2249-2256.

Smith, S. A. & Kuczynski, K. 1978. Observations on the joints of the hand. *The Hand,* 10**,** 226-231.

Sophia Fox, A. J., Bedi, A. & Rodeo, S. A. 2009. The basic science of articular cartilage: structure, composition, and function. *Sports health,* 1**,** 461-468.

Stegmann, M. B. & Gomez, D. D. 2002. A brief introduction to statistical shape analysis. *Informatics and mathematical modelling, Technical University of Denmark, DTU,* 15.

Tan, J., Xu, J., Xie, R. G., Deng, A. D. & Tang, J. B. 2011. In Vivo Length and Changes of Ligaments Stabilizing the Thumb Carpometacarpal Joint. *The Journal of hand surgery,* 36**,** 420-427.

Valdes, K. & Von Der Heyde, R. 2012. An exercise program for carpometacarpal osteoarthritis based on biomechanical principles. *Journal of Hand Therapy,* 25**,** 251-263.

Valero-Cuevas, F. J., Johanson, M. E. & Towles, J. D. 2003. Towards a realistic biomechanical model of the thumb: the choice of kinematic description may be more critical than the solution method or the variability/uncertainty of musculoskeletal parameters. *Journal of biomechanics,* 36**,** 1019-1030.

Van Brenk, B., Richards, R., Mackay, M. & Boynton, E. 1998. A biomechanical assessment of ligaments preventing dorsoradial subluxation of the trapeziometacarpal joint. *The Journal of hand surgery,* 23**,** 607-611.

Van Haver, A., Mahieu, P., Claessens, T., Li, H., Pattyn, C., Verdonk, P. & Audenaert, E. 2014. A statistical shape model of trochlear dysplasia of the knee. *The Knee,* 21**,** 518-523.

Van Nortwick, S., Berger, A., Cheng, R., Lee, J. & Ladd, A. L. 2013. Trapezial topography in thumb carpometacarpal arthritis. *Journal of wrist surgery,* 2**,** 263-270.

Vos, F., De Bruin, P. W., Aubel, J., Streekstra, G. J., Maas, M., Van Vliet, L. J. & Vossepoel, A. M. A statistical shape model without using landmarks. Pattern Recognition, 2004. ICPR 2004. Proceedings of the 17th International Conference on, 2004. IEEE, 714-717.

Wohlman, S. J. & Murray, W. M. 2013. Bridging the gap between cadaveric and in vivo experiments: a biomechanical model evaluating thumb-tip endpoint forces. *Journal of biomechanics,* 46**,** 1014-1020.

Xu, L., Strauch, R. J., Ateshian, G. A., Pawluk, R. J., Mow, V. C. & Rosenwasser, M. P. 1998. Topography of the osteoarthritic thumb carpometacarpal joint and its variations with regard to gender, age, site, and osteoarthritic stage. *The Journal of hand surgery,* 23**,** 454-464.

Zhang, J., Malcolm, D., Hislop-Jambrich, J., Thomas, C. D. L. & Nielsen, P. M. 2014. An anatomical region-based statistical shape model of the human femur. *Computer Methods in Biomechanics and Biomedical Engineering: Imaging & Visualization,* 2**,** 176-185.